Stability of Distribution Systems with a Large Penetration of Distributed Generation

der Fakultät für Elektrotechnik und Informationstechnik

der

Universität Dortmund

genehmigte

DISSERTATION

zur Erlangung des akademischen Grades

Doktor der Ingenieurwissenschaften

von

Bin Huang   M.Sc.(Eng)

Dortmund

Referent: Prof. Dr.-Ing. E. Handschin

Korreferent: Prof. Dr.-Ing. Dr.-Ing. S. Kulig

Tag der mündlichen Prüfung: 9. November 2006

Acknowledgements

Contents

List of the Acronyms

ASPAS	Adaptive Set Point Adjustment Scheme
CCP	Common Coupling Point
CE	Characteristic Eigenvalues
CN	Connecting Node
CRE	Critical Eigenvalues
CRF	Common Reference Frame
DAE	Differential and Algebraic Equations
DG	Distributed Generation
EN	Ending Node
ODE	Ordinary and Differential Equations
OLTC	On Load Tap Changer
PWM	Pulse Width Modulation
SN	Starting Node
SNI	Study Network I
SNII	Study Network II
TN	Trivial Node
UN	Upstream Node
WGS	Wind Generation System

Chapter 1

Introduction

1.1 Motivation and Objectives of this Work

The large increase of distributed generation (DG), which usually means a small-scale power generation located at or near to the load being served, has a large impact on system operations. The growing trend of DG is easily to be recognized because of various political, economic and environmental reasons. In order to be prepared for problems that may happen when the expectation of a high penetration level of DG comes true, huge amount of efforts of power system engineers have been spent in this field.

It is by no means easy to give a general view of the state of the art for the research about DG, because of the prompt evolvement and the various emphases of different researches. In the following, a review is presented by focusing on the works which concern the determination of the allowable penetration level of DG and the impact of DG on the power system stability.

In [1] the authors attempt to determine a wind power penetration constraint based on a worst case wind generation change due to a thunderstorm. The authors of [2] discuss the allowable penetration level of DG from the viewpoint of harmonic distortion prevention, while the authors of [3] study the similar problem by considering another factor – the influence of different excitation system control modes on the integration of distributed synchronous generators. Papers [4][5][6] present the impact of DG on trans-

mission system transient stability, meanwhile, [4][6] also address the transmission system small signal stability. In papers [7][8][9], the influences of DG on system transient stability, voltage stability and voltage quality are discussed. Papers [10][11][12][13] focus mainly on the aspect of islanding operation. In particular, [13] investigate the impact of high wind power penetration on the frequency stability of power systems under islanding conditions. In [14], the selection of switch placement to improve the reliability of radial distribution systems with DG under fault conditions is presented.

As far as the author of this thesis known, to present, the impact of DG on the small signal stability of distribution systems is relatively less to be discussed. From the author's personal viewpoint, the main reasons may be:

- **Possibilities of unsymmetric/unbalanced operations of distribution systems** - Compared to transmission systems, distribution systems are subject to higher potential of unsymmetric or unbalanced operations. However, the effective method of modal analysis for small signal stability mainly reflects the dynamic characteristics of power systems at a specific equilibrium point under the condition of three phase symmetry and balanced operations. These constitute a dilemma.

- **Lack of a general model of DG** - Presently there are several technologies for DG applications, such as wind power plant, solar photovoltaic generation, fuel cells, etc. However, even for a certain technology, similar products from different manufacturers vary quite a lot about their structure and parameters. This makes the task of building a general model of DG a demanding challenge. On the contrary, the small signal stability of the system to a large extent is determined by the eigenvalues of the corresponding linearized model, which heavily depend on the structure and parameter of the system itself. These constitute another dilemma.

Nevertheless, the question has to be answered: to what penetration level of DG can a distribution system be operated without instability problems?

Thus, one of the objectives of this dissertation is to identify if a high penetration level of DG will lead to instability problems in a distribution system. If so, the further step is

proposed as to find a solution to eliminate the resulted instability problems; if not, the further step is proposed as to find some feasible methods to increase the penetration level of DG.

Power system stability mainly includes categories of transient stability, small signal stability, voltage stability and frequency stability. Besides small signal stability, this thesis also gives some discussions about voltage stability. Others, such as transient stability concerning DG and distribution systems, since it has been discussed in many publications, thus will not be addressed here. As for frequency stability, because it will be not very likely to happen just due to the integration of many DG in a rather long time period, thus will not be studied in this work.

When discussing the small signal stability, the following assumptions are adopted:

1. System parameters are three phase symmetric and system operations are three phase balanced. This may be acceptable at least for German grid, since its distribution systems are well planned and structured.

2. Among lots of DG technologies, constant speed wind generation systems are specifically designated to proceed the investigation, since, on the one side, they have a relatively strong interaction with the connected system; on the other side, their mathematically mature model is available.

Another objective of this thesis is to give an answer to the following consideration: Compared to transmission system, disturbances occur in distribution system more often. The connection of DG will make this situation even worse. Hence a reasonable question can be as follows: will these apparently continuous disturbances act as a chain to cause some dangerous events in the electrical network itself (dynamics of other components, such as generators and DG, are not included)?

This question is answered by investigating the relation between the eigenvalues of the state space model of the electrical network and the reasonable expectations of the time interval of two successive disturbances.

The obtained results can simultaneously serve as a verification and validation of the correctness of the network model: As well known, when discussing power system stability, normally the network is mathematically modeled as a constant nodal admittance matrix, i.e., the network is treated in steady state, because its dynamics die out quite fast. Now, facing to a distribution system, since the parameters of the lines/cables differ a lot from those of a transmission system, the assumption is still correct, i.e., the network dynamics are still negligible?

1.2   Outline of the Thesis

Following the introduction given in chapter 1, chapter 2 overviews the technical background of this work, mainly including:

1. the concept and attributes of DG, the state of the art of their technologies and their impacts on system operations.

2. various aspects of power system stability, such as the classification of them, the applicable analysis methods and the available simulation tools.

Chapter 3 focuses solely on the dynamics of the electrical network (without other dynamic components, such as synchronous generators, induction motors, etc). The whole network model is built under $dq0$ reference frame after a discussion of the relations between the abc and $dq0$ coordinations. Consequently the network dynamics are studied by evaluating the eigenvalues of the corresponding state matrix.

Chapter 4 investigates the small signal stability of the whole system based on modal analysis when the penetration level of DG achieves a high extent.

Chapter 5 concentrates on the influence of DG and its operation modes on the voltage stability. During the study, the continuation power flow method is adopted to determine the system loadability under different scenarios.

Finally, chapter 6 summarizes the whole work and points out the potential directions for future research.

Chapter 2

Concepts, Attributes and Technologies of Distributed Generation and Power System Stability

2.1 Distributed Generation

2.1.1 Concept and Attributes of Distributed Generation

During the past several decades, power generation has been highly centralized in large power plants. Customers are served primarily by utility distribution companies that have connections to large generation facilities using high-voltage transmission lines and connections to customers through their lower-voltage distribution lines.

This operating structure is built on the basis of economy, security, and quality of supply. It is operated by hierarchical control centers and allows the system to be monitored and controlled continuously. The generation is instantly adjusted to the consumption by monitoring the frequency and on the basis of elaborated load forecasting models. The voltage is controlled to be within specific limits by means of appropriate coordinated devices, generators, on load tap changers (OLTC), reactive compensation devices, etc.

Nowadays there is a considerable interest in connecting generation to the distribution system and this is termed as DG.

Compared to conventional generation, DG usually has characteristics as [15][16]:

- not centrally planned
- not centrally dispatched
- with small capacity
- usually connected to the distribution system.

And it mainly contributes to [15][16]:

- reduction of emission levels (mainly CO_2)
- energy efficiency or rational use of energy
- deregulation or competition policy
- diversification of energy sources
- ease of finding sites for smaller generators
- short construction times and lower capital costs of smaller plant
- reduction of power transmission costs and losses.

2.1.2   Overviews of Distributed Generation Technology

The currently available DG technologies up to a capacity of 5 MW, mainly include [17]:

- **Microturbines** - This new and emerging technology is currently only available from a few manufacturers. Other manufacturers are looking to enter this emerging market, with models ranging from 30 to 200 kW. Microturbines promise low emission levels, but the units are currently relatively expensive. Obtaining reasonable costs and demonstrating reliability will be major hurdles for manufacturers. Microturbines are just entering the marketplace, and most installations are for the purpose of testing the technology.

- **Industrial combustion turbines** - This mature technology ranges from 1 MW to over 5 MW. They have low capital cost, low emission levels, but also usually low electric efficiency ratings. Development efforts are focused on increasing efficiency levels for this widely available technology. Industrial combustion turbines are being used primarily for peaking power and in cogeneration applications.

- **Fuel cells** - Although the first fuel cell was developed more than 150 years ago, this technology remains in the development stage. Fuel cell emission levels are quite low, but cost and demonstrated reliability remain major problems for its market penetration. The few fuel cells currently being used provide premium power or are in applications subsidized by the government or gas utilities.

- **Photovoltaics** - Commonly known as solar panels, photovoltaic (PV) panels are widely available for both commercial and domestic use. Panels range from less than 5 kW and up to several MW. They produce no emissions, and require minimal maintenance. However, they can be quite costly. Less expensive components and advancements in the manufacturing process are required to eliminate the economic barriers now impeding the wide-spread use of PV systems. Photovoltaics may be used in remote locations without grid connections.

- **Wind turbine systems** - Wind turbines are currently available from many manufacturers. Compared to other renewable technologies, they provide a relatively inexpensive way to produce electricity. But as relying upon the variable and somewhat unpredictable wind, they are not suited for continuous power production.

2.1.3   Impact of Distributed Generation to Power System Operation

From a technical aspect, DG poses some impacts on power systems, especially to the operations of distribution systems. They mainly include [15][16][18]:

- **Voltage Issue** - The utility must provide electricity to the customers at a voltage within specific limits. However, if the capacity of the connected DG is relatively large or the connection between transmission and distribution system is relatively weak, the steady state voltage rise may be a problem.

- **Protection** - The connection of DG changes the magnitude, duration, and direction of a fault current, thus requires corresponding adaptations of the existing protection system.

- **Power Quality** - Most commonly recognized power quality events include frequency fluctuation, sustained over voltages, high frequency noise, harmonic distortions, high voltage spikes and voltage sags and swells. DG may decrease the power

quality when it has relatively large capacity or is connected to a weak distribution
system.

- **Stability** - The increment of the capacity of DG determines that it plays a more and
  more important role in power system stability. Therefore more considerations are
  required in this aspect.

- **Security** - DG energizes the system via lots of points thus complicates the policies
  of isolation and earthing for safety before maintenance work is undertaken.

2.2   Power System Stability

2.2.1   Overview of Power System Dynamics

In order to gain a better understanding of power system stability, some knowledge of the
dynamic phenomena in power system is necessary. Dynamics here means the character-
istics of the way the power system responds to a disturbance. Such a disturbance can be
either an intentional operation, e.g., a scheduled generator switching, or an accident, e.g.,
a light striking. One of the common and perhaps most important classification of power
system dynamics is their natural time range of response. There are various categorizations
of power system dynamic phenomena by considering them in different levels of detail. In
this work, the classification given in [19] is adopted.

Power system dynamics can be divided into four groups as shown in fig. 2.1. Among
them, *wave dynamics*, or surges, are the fastest dynamics, which occur in high volt-
age transmission lines and result from the propagation of electromagnetic waves caused
by lightning strikes or switching operations. Slower are the *electromagnetic dynamics*,
which take place in the machine windings following a disturbance. Much slower are the
electromechanical dynamics, which describe the oscillation of the rotating masses of gen-
erators and motors when the system is subject to disturbances. Thermodynamics are the
slowest ones which correspond to phenomena such as boiler control action in steam power
plants as a response to frequency variations. In the following sections, the discussed
problems of power system stability mainly belong to the categories of electromechanical
dynamics and thermodynamics, i.e., they vary from seconds to many minutes.
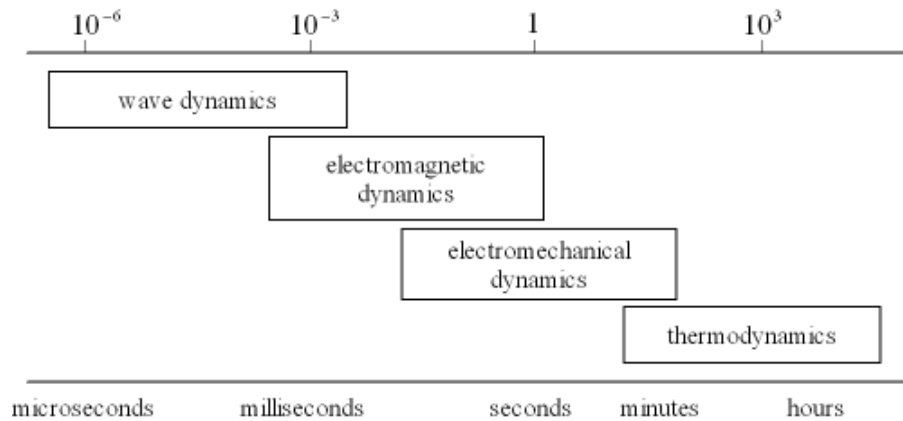
Figure 2.1: Time range of power system dynamics [19]

2.2.2   Concepts and Methods for Analyses of Power System Stability

Stability, as a fundamental concept in most engineering disciplines, has been extensively studied and more than 28 definitions of it are introduced in the system theory focused on different technical and physical aspects. In power system engineering, the proposed definition, in a recent work of IEEE/CIGRE Joint Task Force [20], is formed as:

- *Power system stability is the ability of an electric power system, for a given initial operating condition, to regain a state of operating equilibrium after being subjected to a physical disturbance, with most system variables bounded so that practically the entire system remains intact.*

In the early stage, power system engineers mainly encountered instability problems related to generator rotor angle stability, with which the whole system can not keep synchronism after a disturbance. However, with the continuous expansion of modern power systems under more stressed operation conditions, different forms of system instability have emerged.

A more detailed classification according to the different mechanism is helpful to understand the problems well, though the power system stability is essentially a single problem. In [20], three categories have been proposed, i.e., rotor angle stability, voltage stability and frequency stability.

Rotor Angle Stability

Rotor angle stability refers to the ability of synchronous machines of an interconnected power system to remain in synchronism after being subjected to a disturbance. It depends on the ability to maintain/restore equilibrium between electromagnetic torque and mechanical torque of each synchronous machine in the system. Instability that may result occurs in the form of increasing angular swings of some generators leading to their loss of synchronism with other generators [20].

By considering the size of the disturbance, it can be further divided into two subcategories:

- Small disturbance rotor angle stability, sometimes also referred to as small signal stability, is concerned with the ability of the power system to maintain synchronism under small disturbances, such as a small load increment. Small signal stability depends on the initial state of the system. In today's power systems, small signal instability problems are usually caused by the lack of enough damping torque, under which some variables of the power system show an oscillation characteristics with increasing amplitude after being subjected to a disturbance.

  Since the disturbance is assumed to be small, the linearization of system model is allowable and thus the modal analysis methods are applicable [21][22][23]. Nonlinear time domain simulation is another effective approach in the analysis of the small signal stability problems. The results of modal analysis usually have to be verified by using the time domain simulations as a benchmark. However, the simulation method has relatively weak ability to determine the critical modal characteristics, which is important for designing appropriate countermeasures; while the modal analysis gives complete information on the inherent characteristics of modes (mode shapes, participation factors, transfer functions, etc.), which can be used in control design for damping enhancement. A feasible proposal is to use both of them in a complementary manner [24]. Besides, bifurcation theory is applicable by noticing that the small signal stability is bounded by the occurrence of Hopf bifurcation (where a pair of complex-conjugate eigenvalues of the system appears) [25][26].

- Large disturbance rotor angle stability, sometimes also named as transient stability, is concerned with the ability of the power system to maintain synchronism when subjected to a severe disturbance, such as a short circuit on a transmission line. Transient stability depends on both the initial operating state of the system as well as the severity of the disturbance. Instability problems are usually due to insufficient synchronizing torque thus evolve normally in the form of aperiodic angular deviations.

The highly nonlinear characteristics of transient stability decide that the nonlinear time domain simulation will play an important role in relevant studies. This simulation is actually a numerical procedure to solve the differential and algebraic equations (DAE) of a power system [21][27]. Another way to determine the stability is the so called direct method, in which a Lyapunov function is formed and thus Lyapunov's second method is adopted for the evaluation. However, this method mainly has two difficulties: 1. How to construct a good Lyapunov function; 2. How to assess a practical stability domain [21][27][28]. Further, methods based on pattern recognition are also proposed for transient stability analysis, which try to infer results about the present stability properties by digging information from the "past experience" [27].

Voltage Stability

Voltage stability refers to the ability of a power system to maintain steady voltages at all buses in the system after being subjected to a disturbance from a given initial operating condition. It depends on the ability to maintain/restore equilibrium between load demand and load supply from the power system. Instability that may results occurs in the form of a progressive fall or rise of voltages of some buses. A possible outcome of voltage instability is loss of load in an area, or tripping of transmission lines and other elements by their protective systems leading to cascading outages [20].

The loads are usually the driving force for voltage instability. When subjected to a disturbance, the power consumption of the loads tends to be restored due to the action of OLTC, thermostats, etc. This leads to the reactive power consumption increment thus

further voltage reduction. A progressive drop of the voltage persists which finally results in voltage collapse, when there is no enough generator capability or network transfer capacity available. The network transfer capacity is determined by the voltage level and the magnitude of the corresponding impedance [21][29].

As in transient stability analysis, time domain simulation also serves as an effective and accurate tool for analyzing voltage stability. However the computation requirement is demanding. In order to speed the analysis, some simplifications are made by assuming the system in a steady state thus those static methods are applicable, such as using continuation method to determine the loadability limits and adopting some sensitivity index to estimate the distance from the present system operation point to the voltage collapse point [21][29][30]. Bifurcation analysis is also appropriate for voltage stability since it is observed that the instability that may occur usually coincides with the singularity of system state Jacobian, which is the necessary condition of saddle-node bifurcation [29].

Frequency Stability

Frequency stability refers to the ability of a power system to maintain steady frequency following a severe system upset resulting in a significant imbalance between generation and load. It depends on the ability to maintain/restore equilibrium between system generation and load, with minimum unintentional loss of load. Instability that may result occurs in the form of sustained frequency swings leading to tripping of generating units and/or loads [20].

The possible instability is usually analyzed with time domain simulation. Though the procedure is similar as that in transient stability simulation, the model of the power system may need some adaptation. For example, since the potential frequency instability is usually a long term dynamic process after the system being subjected to a severe upset, proper representations of the prime mover, energy supply systems and functions of wide range protection and control systems may be necessary [21].

Comments on Classification

The classification of power system stability helps identifying causes of instability, applying suitable analysis tools, and developing corrective measures. However, in a real situation any one form of instability may not occur solely. This is true especially for highly stressed systems and for cascading events. Thus power system stability will by all means be considered as a whole; no category of the mentioned stability would be bettered at the expense of another [20].

2.2.3   Simulation Tools for Analyses of Power System Stability

Nowadays many powerful software packages are available for analyses of power system stability. Some of them are mature and commercial tools, while the others are useful and open source programs.

PSAT, a freely distributed Matlab-based power system analysis program developed by Dr. Federico Milano [31], stands out among those open source and freely available programs for its relatively complete functionalities. It includes functions as power flow, continuation power flow, optimal power flow, small-signal stability analysis, and time-domain simulation. To fulfill these analyses, PSAT supports a variety of static and dynamic models. For example, in a static analysis, a synchronous generator can be modeled as a slack bus or a PV bus; however, in a dynamic analysis, options of the synchronous generator model with a dynamic order varying from 2 to 8 are provided. Besides, PAST includes a user friendly graphical interface and a Simulink-based one-line network editor [32].

These characteristics make PSAT attractive thus be adopted for the work presented in this thesis. During the research, all concerned codes have been carefully investigated. Some small errors have been fixed and some models have been adapted/developed. About these aspects, more details are given in following chapters.

Chapter 3

Study of the Eigenvalues of the State Space Model of Distribution Networks

Network dynamics are normally omitted in order to simplify power system stability analysis. This is based on the observation that the components of power systems have quite different time constant of the natural response, for which a general view is given in [33]. [34] further justifies the elimination of network transients in power system stability analysis via using singular perturbation theory. Though papers [35][36][37] put forward suggestions and accompanying reasons of including network dynamics into a large scale analysis, considering this will prominently increase the dynamic order of the studied system, the feasibility of it is still open for more investigations.

The necessity of including network dynamics is studied in this thesis based on the following observations: firstly, the trend of integrating more and more DG into the present power systems is well recognized; secondly, compared to traditional electricity sources/loads connected to the distribution network, these DG have a relatively large capacity up to several megawatt; last but not least, the operation of DG has more or less some stochastic properties, for which the output of wind generation systems or photovoltaic systems may serve as an example. All these combined together, leads to the question studied here, i.e., if the incessant stochastic inputs (power, currents ... etc.) will act as a chain to induce harmful responses (nodal overvoltage ... etc.) in the distribution network? This question has been investigated in this chapter by analyzing the properties of the eigenvalues of the distribution network state space model.

In this chapter, section 3.1 focuses on modeling lines/cables in $dq0$ reference frame. Section 3.2 introduces a method to form the state space model of a distribution network. Information about the study networks is given in 3.3, while section 3.4 presents simulations, results and comments.

The reason of modeling the network in $dq0$ reference frame is, if the analysis results demonstrate that the negligence of the distribution network dynamics is inappropriate, the developed models and programs can be directly incorporated to other system component models for the consequent analysis.

Main conclusions of this chapter are:

1. For distribution networks, since generally the dynamics die out quite fast, the apparently successive stochastic disturbances have nearly independent influences on the network. Hence these impacts can be studied independently.

2. It is not necessary to include the electric network dynamics into the stability analysis. The distribution network can still be mathematically modeled via a nodal admittance matrix.

3.1 Modeling of Lines/Cables

3.1.1 Selection of a Common Reference Frame

The introduction of Park Transformation simplifies the mathematical description of synchronous machines. It defines a new set of stator variables such as currents and voltages, which are obtained by projecting the actual variables on abc axes to $dq0$ axes. However, during the analysis, each synchronous machine is modeled in its own $dq0$ reference frame. When simulating an interconnected system, all the variables have to be referred to a common reference frame (CRF). After the determination of the CRF, other system variables and component models, e.g., models of induction motors, normally are also referred to this frame to simplify the analysis [21][38][39].

To build the model of the electrical network under $dq0$ frame, Kron transformation [40] is adopted. In this work, the reference frame of Kron transformation is selected the same as the CRF which is specifically designated as: in which, the q axis leads the d axis by $90°$ and coincides with the system reference phasor, as shown in fig. 3.1.
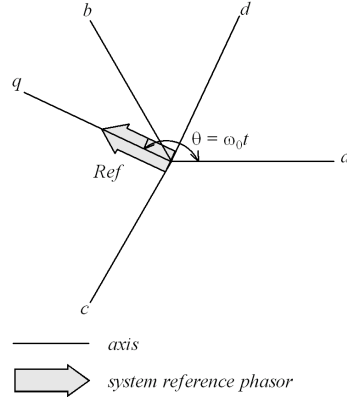
Figure 3.1: Selection of the common reference frame

Hence the transformation matrix from *abc* reference frame to $dq0$ reference frame is

$$\mathbf{P} = \frac{2}{3} \begin{bmatrix} \sin\theta & \sin(\theta - \frac{2\pi}{3}) & \sin(\theta + \frac{2\pi}{3}) \\ \cos\theta & \cos(\theta - \frac{2\pi}{3}) & \cos(\theta + \frac{2\pi}{3}) \\ \frac{1}{2} & \frac{1}{2} & \frac{1}{2} \end{bmatrix} \tag{3.1}$$

where

$\theta = \omega_0 t$, $\omega_0 = 2\pi f$, f the system frequency.

The inverse transformation matrix is

$$\mathbf{P}^{-1} = \begin{bmatrix} \sin\theta & \cos\theta & 1 \\ \sin(\theta - \frac{2\pi}{3}) & \cos(\theta - \frac{2\pi}{3}) & 1 \\ \sin(\theta + \frac{2\pi}{3}) & \cos(\theta + \frac{2\pi}{3}) & 1 \end{bmatrix} \tag{3.2}$$

3.1.2 Relation of Network Eigenvalues under *abc* and $dq0$ Frames

To investigate the properties of network dynamics by evaluating the eigenvalues of the network under $dq0$ frame, the theoretical precondition is that the eigenvalues under *abc* frame can be reconstructed from those under $dq0$ frame. This can be achieved based on the following observation:

Observation

Assuming a symmetric network has $3N$ state variables, thus it has $3N$ eigenvalues. Under *dq*0 reference frame, these $3N$ eigenvalues consist of N pairs of eigenvalues which are complex-conjugate/double-real ones and relate only to the *dq* components (lately referred to as λ_{dq}), and N eigenvalues which relate only to the 0 components (lately referred to as λ_0). Correspondingly, under *abc* frame the $3N$ eigenvalues can also be divided into two groups, one of which contains N pairs of eigenvalues (lately referred to as λ_{abc2N}), the other includes the rest (lately referred to as λ_{abcN}). Then the eigenvalues of the network model in *abc* and *dq*0 reference frame have the following relations:

- For λ_{abc2N}, assuming it includes complex-conjugate eigenvalues $\sigma_1 \pm j\omega_1$, after *dq*0 transformation, the corresponding complex-conjugate eigenvalues will be $\sigma_1 \pm j(\omega_1 - \omega_0)$ and $\sigma_1 \pm j(\omega_1 + \omega_0)$.

- For λ_{abcN}, this set of eigenvalues will keep unchanged after *dq*0 transformation.

Explanation

Reference [40] describes the relations of the eigenvalues of electrical networks under *abc* and *dq*0 frames. But the discussion is just confined to the basic network components such as a series impedance and a shunt capacitance. A general conclusion is not available if the relations presented above are applicable to a much more general and complicate network, for example, the one given in fig. 3.6.

It can be foreseen that a strictly mathematic proof may be too complicated and arduous to achieve. In this thesis, this question is discussed from another aspect, which is much more based on a physical meaning rather than a mathematical reasoning.

The discussion consists of two steps.

- Step 1
  The set of λ_{abc2N} is assumed to have complex-conjugate eigenvalues $\sigma_1 \pm j\omega_1$ (from the later example it can be seen these complex-conjugate eigenvalues usually appear as two pairs).

Firstly, the input signals $\mathbf{I}_{abc}$ in fig. 3.2 are assumed to be positive sequential sinusoids with frequency of ω_1. It is well known that when the input signals are applied to the network at $t = 0$, the output signals $\mathbf{O}_{abc}$ can be considered as a combination of transient signals as well as steady signals. The transient signals will die out as time is passing, while the steady signals will exist as long as the input signals sustain. The amplitude of the steady signals are determined by both the poles and the zeros of the system. For simplifying the discussion, it is assumed the steady output signals have a prominently large amplitude, i.e., there exists a resonance in the responses. It can be shown that after $dq0$ transformation, the input signals $\mathbf{I}_{dq0}$ in fig. 3.2 consist of only dq components, which are sinusoidal signals with frequency of $\omega_1 - \omega_0$, while the 0 component constantly equals to zero [41]. Meanwhile, when applying $dq0$ transformation to the outputs signals $\mathbf{O}_{abc}$, which is equivalent to apply the transformation separately to the transient signals as well as the steady signals in $\mathbf{O}_{abc}$, this leads to: for the transient signals, their decaying ratio will keep unchanged, which means the real parts of the eigenvalues hold unchanged; for the steady signals, the frequency will be shifted to $\omega_1 - \omega_0$, which means under $dq0$ frame the resonance frequency is shifted from ω_1 to $\omega_1 - \omega_0$. Combining these together indicates that the network model under $dq0$ frame has eigenvalues at $\sigma_1 \pm j(\omega_1 - \omega_0)$.

Then negative sequential sinusoids with frequency of ω_1 are assumed to be the input signals $\mathbf{I}_{abc}$. It is noted that the negative sequence signals have nearly the same impact to the network as that of the positive sequence signals. Following a similar reasoning as mentioned above, it can be found that the network model under $dq0$ frame has eigenvalues at $\sigma_1 \pm j(\omega_1 + \omega_0)$.

It is worth noting that the $dq0$ transformation will also alter the frequency of the transient signals. However, in above discussions the attention is only focused on the alteration of the decaying ratio of the transient signals. This may help to make the discussions easier.

- Step 2

Suppose that the set of λ_{abcN} has complex conjugate eigenvalues $\sigma_2 \pm j\omega_2$ and the input signals $\mathbf{I}_{abc}$ are three phase identical (zero sequence) and sinusoidal with frequency of ω_2. A similar deduction procedure as in step 1 reveals that the eigenvalues hold the same under *abc* and *dq*0 frames.

It may help to note that during the deduction, the application of *dq*0 transformation to three phase identically sinusoidal signals will lead to zero in *dq* axis while a sinusoidal signal the same as the input signal in 0 axis.
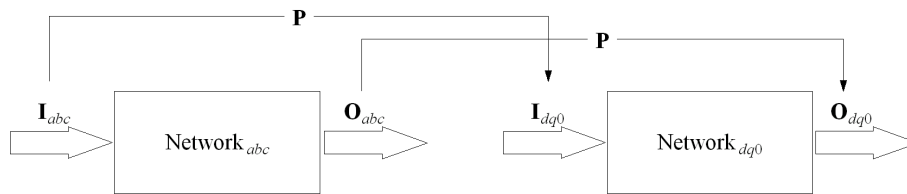
Figure 3.2: System under *abc* and *dq*0 frames

Example

A small network shown in fig. 3.3 is used to illustrate the given observation. Its parameters are as follows:

Impedance

Node	Node	R_s	R_m	L_s	L_m
1	2	0.02	0.012	0.2	0.1
2	3	0.04	0.01	0.35	0.18
3	4	0.08	0.035	0.27	0.13
3	5	0.1	0.06	0.5	0.23

Capacitance

Node	C_s	C_m
2	0.01	0.002

The eigenvalues under *abc* and *dq*0 frames are given in table 3.1.
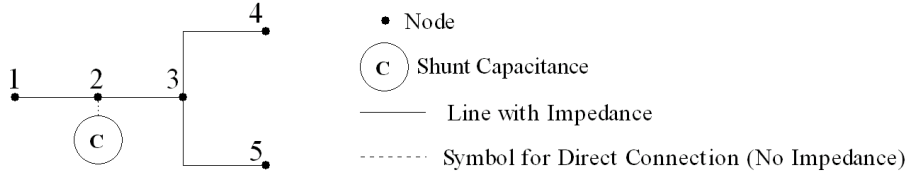
Figure 3.3: Example for investigating the network eigenvalues under *abc* and *dq*0 frames

λ_{abc}	λ_{abc2N}	$-18.058 \pm j13055$	$-18.058 \pm j13055$	-73.708
		-73.708	-45.355	-45.355
	λ_{abcN}	$-18.697 \pm j4932.4$	-78.436	-41.588
λ_{dq0}	λ_{dq}	$-18.058 \pm j13369$	$-18.058 \pm j12740$	$-73.708 \pm j314.16$
		$-45.355 \pm j314.16$		
	λ_0	$-18.697 \pm j4932.4$	-78.436	-41.588

Table 3.1: Eigenvalues of the system given in fig. 3.3

3.1.3   Modeling Lines/Cables in *dq*0 Reference Frame

Before deducing the network dynamic model, the lines/cables are modeled in advance.

A single phase equivalent of a serial impedance is shown in fig. 3.4(*a*). In *abc* frame, it is described by

$$\mathbf{L}\frac{d\mathbf{I}_{abc}}{dt} + \mathbf{R}\mathbf{I}_{abc} = \mathbf{V}_{1abc} - \mathbf{V}_{2abc} \tag{3.3}$$

where $\mathbf{I}_{abc} = [i_a\ i_b\ i_c]^T$, $\mathbf{V}_{abc} = [v_a\ v_b\ v_c]^T$. The superscript T means transpose. Besides, since the network is assumed to be symmetric, thus $\mathbf{L}$ and $\mathbf{R}$ are

$$\mathbf{L} = \begin{bmatrix} L_s & L_m & L_m \\ L_m & L_s & L_m \\ L_m & L_m & L_s \end{bmatrix}, \mathbf{R} = \begin{bmatrix} R_s & R_m & R_m \\ R_m & R_s & R_m \\ R_m & R_m & R_s \end{bmatrix}$$

where

L_s is the self inductance, L_m the mutual inductance

R_s the self resistance, R_m the mutual resistance

Similarly, a single phase equivalent of a shunt capacitance is shown in fig. 3.4(*b*). It

is described by

$$\mathbf{C}\frac{d\mathbf{V}_{abc}}{dt} = \mathbf{I}_{1abc} - \mathbf{I}_{2abc} \tag{3.4}$$

with

$$\mathbf{C} = \begin{bmatrix} C_s & C_m & C_m \\ C_m & C_s & C_m \\ C_m & C_m & C_s \end{bmatrix}$$

where C_s is the self capacitance, C_m the mutual capacitance.

(a)

(b)
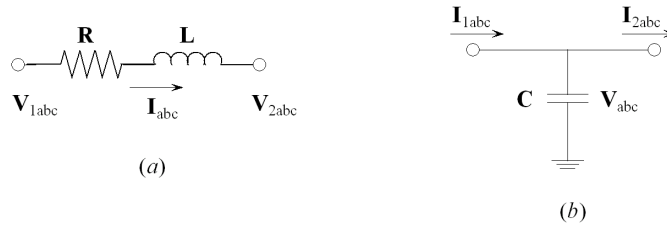
Figure 3.4: Single line diagram of basic components of lines/cables

By applying Kron transformation to eqn. (3.3) leads to

$$\mathbf{PL}\frac{d(\mathbf{P}^{-1}\mathbf{I}_{dq0})}{dt} + \mathbf{PRP}^{-1}\mathbf{I}_{dq0} = \mathbf{V}_{1dq0} - \mathbf{V}_{2dq0} \tag{3.5}$$

As discussed in [41], eqn. (3.5) can be rearranged as

$$\begin{aligned} L\frac{di_d}{dt} - \omega_0 L i_q + R i_d &= v_{1d} - v_{2d} \\ L\frac{di_q}{dt} + \omega_0 L i_d + R i_q &= v_{1q} - v_{2q} \\ L_0\frac{di_0}{dt} + R_0 i_0 &= v_{10} - v_{20} \end{aligned} \tag{3.6}$$

where

$$L = L_s - L_m, \quad L_0 = L_s + 2L_m$$
$$R = R_s - R_m, \quad R_0 = R_s + 2R_m$$

By applying Kron transformation to eqn. (3.4) leads to

$$\mathbf{PC}\frac{d\mathbf{P}^{-1}\mathbf{V}_{dq0}}{dt} = \mathbf{I}_{1dq0} - \mathbf{I}_{2dq0} \tag{3.7}$$

which can be rearranged as

$$
\begin{aligned}
C\frac{dv_d}{dt} - \omega_0 C v_q &= i_{1d} - i_{2d} \\
C\frac{di_q}{dt} + \omega_0 C v_d &= i_{1q} - i_{2q} \\
C_0\frac{dv_0}{dt} &= i_{10} - i_{20}
\end{aligned}
\tag{3.8}
$$

where

$$
C = C_s - C_m, \quad C_0 = C_s + 2C_m
$$

When choosing the following base quantities for the variables in $dq0$ frame

v_b = peak value of rated line-to-neutral voltage, V

i_b = peak value of rated line current, A

f_b = rated frequency, Hz

Then the per unit equations of eqn. (3.6) is:

$$
\begin{aligned}
\frac{\bar{L}}{\omega_0}\frac{d\bar{i}_d}{dt} - \bar{L}\bar{i}_q + \bar{R}\bar{i}_d &= \bar{v}_{1d} - \bar{v}_{2d} \\
\frac{\bar{L}}{\omega_0}\frac{d\bar{i}_q}{dt} + \bar{L}\bar{i}_d + \bar{R}\bar{i}_q &= \bar{v}_{1q} - \bar{v}_{2q} \\
\frac{\bar{L}_0}{\omega_0}\frac{d\bar{i}_0}{dt} + \bar{R}_0\bar{i}_0 &= \bar{v}_{10} - \bar{v}_{20}
\end{aligned}
\tag{3.9}
$$

where the super bar denotes a per unit variable.

Similarly the per unit equation of (3.8) is

$$
\begin{aligned}
\frac{\bar{C}}{\omega_0}\frac{d\bar{v}_d}{dt} - \bar{C}\bar{v}_q &= \bar{i}_{1d} - \bar{i}_{2d} \\
\frac{\bar{C}}{\omega_0}\frac{d\bar{v}_q}{dt} + \bar{C}\bar{v}_d &= \bar{i}_{1q} - \bar{i}_{2q} \\
\frac{\bar{C}_0}{\omega_0}\frac{d\bar{v}_0}{dt} &= \bar{i}_{10} - \bar{i}_{20}
\end{aligned}
\tag{3.10}
$$

Since the system is assumed to operate under balanced conditions, the zero sequence voltages and currents in eqn. (3.9) and (3.10) keep to trivial thus the corresponding equations

are dropped. This leads to

$$\frac{L}{\omega_0}\frac{di_d}{dt} - Li_q + Ri_d = v_{1d} - v_{2d}$$
$$\frac{L}{\omega_0}\frac{di_q}{dt} + Li_d + Ri_q = v_{1q} - v_{2q} \tag{3.11}$$

and

$$\frac{C}{\omega_0}\frac{dv_d}{dt} - Cv_q = i_{1d} - i_{2d}$$
$$\frac{C}{\omega_0}\frac{di_q}{dt} + Cv_d = i_{1q} - i_{2q} \tag{3.12}$$

where the super bar is dropped to make the expressions concise.

3.2   Forming of the State Matrix of Distribution Networks

[42] and [43] have introduced some general algorithms of obtaining the state matrix of a
general circuit. Although they are capable of treating the electrical network of a power
system, the development of such a program is not an easy work. In this thesis, the specif-
ically studied object is distribution networks, which normally are weakly meshed. Based
on this attribute, a special way of forming the state matrix is proposed.

The implementation of the proposed method is explained with the simple network shown
in fig. 3.5. An assumption is adopted here that in the example between two nodes there ex-
ists only an impedance. The capacitance of the lines/cables will be presented and treated
as an independent shunt component.

The procedure consists of six steps as:

Step 1, Nodal Characteristics Analysis
For a distribution network, three kinds of nodes are important for the analysis. They are:

1. Starting Node (SN). SN is usually the common coupling point (CCP) of a transmis-
   sion network and a distribution network. In fig. 3.5, node 1 is the SN.

2. Ending Node (EN). EN is a node where only one transmission line is connected. In
   fig. 3.5, node 7, 8, 9, 10 and 11 are EN.
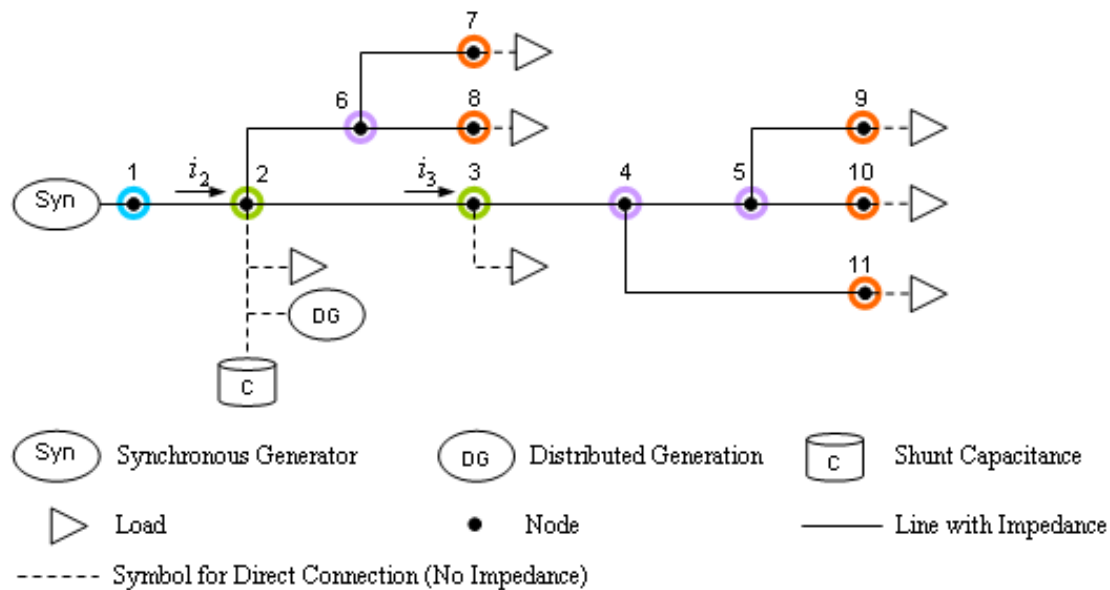
Figure 3.5: Example for explanation of the procedure to form network state matrix

3. Connecting Node (CN). CN is a node which connects at least two lines/cables as well as other energy sources/sinks (such as DG, shunt capacitors, loads, etc). In fig. 3.5, node 2 and 3 are CN. It is worth noting that though node 4, 5 and 6 connect also more than one transmission lines, they are not CN since there is no other energy sources/sinks connected to them.

Besides these, for convenience of the subsequent illustration, all remaining nodes will be referred to as Trivial Node (TN). In fig. 3.5, node 4, 5, 6 are TN.

Step 2, The Selection of State Variables

After the determination of SN, EN CN and TN, the state variables of the network are specifically designated as:

1. Currents injected into CN and EN. For example, the current flows from node 1 to node 2 will be designated as a state variable and will be briefly named as i_2 rather than i_{12}. Then for state variable i_3 it denotes the current flowing from node 2 to 3. Besides, the definition of the positive direction of the current, for energy sources is that of flowing out, for energy sinks that of flowing in, for transmission lines that of conforming to a general direction of SN → CN → EN.

2. Voltages of the nodes which have a shunt capacitance branch. In fig. 3.5 only the voltage of node 2 is chosen as one of the state variables.

Step 3, Nodes Subgrouping

Then the whole network can be divided into subgroups which include the following nodes:

1. CN and EN which are connected upstream via some common TN to a specific CN.

2. The specific CN itself. Afterwards this node will sometimes be referred to as Upstream Node (UN).

In fig. 3.5, there exist four subgroups, i.e., (1,2), (2,3), (2,7,8), and (3,9,10,11).

Step 4, Forming a General Form for the Differential Equations of the State Variables of Branch Currents

For the above mentioned subgroups, as shown in appendix A, each can be described by a generalized form of differential equations as:

$$\dot{\mathbf{I}}_{2(n-1)\times 1} = \mathbf{A}_{2(n-1)\times 2(n-1)}\mathbf{I}_{2(n-1)\times 1} + \mathbf{B}_{2(n-1)\times 2}\mathbf{v}_{2\times 1} + \mathbf{C}_{2(n-1)\times 2(n-1)}\mathbf{V}_{2(n-1)\times 1} \quad (3.13)$$

where

n is the number of the nodes of respective groups;

$\mathbf{I}$ consists of d, q components of the state variables of the currents of the corresponding group;

$\mathbf{v}$ are the d, q components of the nodal voltage of related UN. $\mathbf{V}$ contains the d, q components of the nodal voltage of that group except the UN.

For example, for group (2,7,8), $\mathbf{I}$ is $[i_{7d}\ i_{7q}\ i_{8d}\ i_{8q}]^T$, $\mathbf{v} = [v_{2d}\ v_{2q}]^T$, and $\mathbf{V} = [v_{7d}\ v_{7q}\ v_{8d}\ v_{8q}]^T$.

Step 5, Forming a General Form for the Differential Equations of the State Variables of Nodal Voltages

For the nodes with a shunt capacitance, they also have a generalized form of differential equations as:

$$\dot{\mathbf{V}}_{2\times 1} = \mathbf{A}_{2\times 2}\mathbf{V}_{2\times 1} + \mathbf{B}_{2\times 2}\sum \mathbf{I} \qquad (3.14)$$

where

V are the d, q components of the nodal voltage;

$\sum \mathbf{I}$ is the summation of the currents flowing in/out the node except the one which flows through the shunt capacitance branch itself.

Taking node 2 as an example, where **V** is $[v_{2d} v_{2q}]^T$, and $\sum \mathbf{I}$ equals

$$
\begin{bmatrix}
i_{2d} + i_{2DGd} - i_{7d} - i_{8d} - i_{3d} - i_{2Loadd} \\
i_{2q} + i_{2DGq} - i_{7q} - i_{8q} - i_{3q} - i_{2Loadq}
\end{bmatrix}
$$

Step 6, If Necessary, Interfacing the Electrical Network Model with Other System Components

Equations (3.13) and (3.14) give enough information about the dynamics of the network. If necessary, a complete system dynamic model can be formed after interfacing them with the dynamic models of other components, such as generators, DG, etc.

3.3   A Brief View of the Study Networks

In this work, two networks are available for the investigation as:

- **Study Network I (SNI)** —- which is presented in fig. 3.6. Its structure is based on IEEE 34 node test feeder [44][45]. Meanwhile, in order to make the network proper for the study of this thesis, some modifications are adopted as follows

    1. The two voltage regulators sited in line segment 814-850 and 852-832 respectively are omitted. The transformer sited in line segment 832-888 is replaced by a line with the length of 1 km.

    2. All lines are assumed to be symmetric.

    3. All loads are assumed to be three phase balanced. Distributed loads are substituted by equivalent spot loads. In general, the magnitudes of the loads are raised up to about ten times bigger than those in the original case.

    More detailed information is given in appendix B.
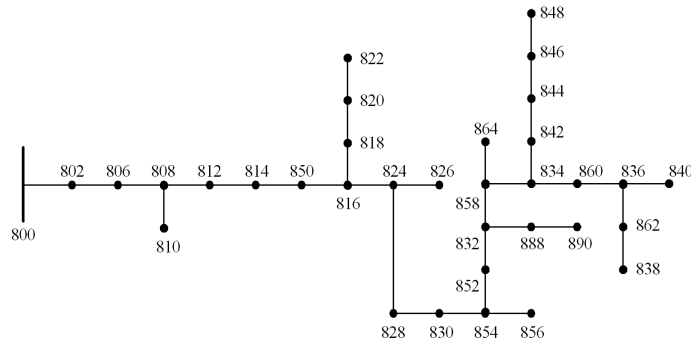
Figure 3.6: Topology of the SNI

- **Study Network II (SNII)** —- which is presented in fig. 3.7. The structure and relevant data are from a real distribution system in Germany. It is worth noting that this network is connected to the transmission system through both node 1 and node 2. More detailed information is given in appendix C.
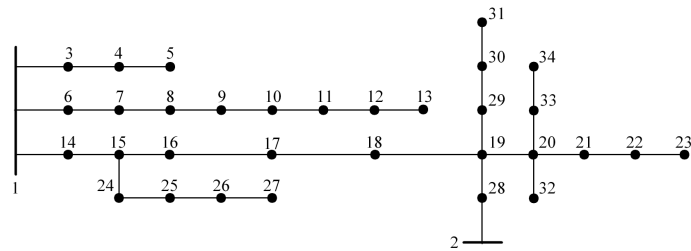
Figure 3.7: Topology of the SNII

In the following parts of this thesis, all the proposed methods and analyzing procedures are explained in detail based on the study of the SNI. However, the obtained conclusions in the stage of studying the SNI will be verified by the study of the SNII.

3.4 Simulations and Results

3.4.1 Properties of Network Eigenvalues

Before turning to further analysis, the term 'Characteristic Eigenvalues' (CE) is introduced in advance. Then the distribution of the CE of the SNI and its variants is investigated. Finally the obtained conclusions are verified by studying the distribution of the CE of the SNII.

Concept of the Characteristic Eigenvalues

Fig. 3.8(a) presents a very simple system: a load is fed by a generator via a transmission line. For the transmission line, if it has the parameters given in appendix B while with the length as 1km, then its π equivalent model will have nine eigenvalues under abc frame as given in fig.3.8(b), which can be separated into two sets, i.e., λ_{abc2N} and λ_{abcN}. Since assuming a balanced operation, only the dq circuit components are included to form the state matrix of the network, thus the corresponding eigenvalues only include λ_{dq}, the counterpart of the set λ_{abc2N}. The set of λ_{abc2N} can be reconstructed from λ_{dq} while λ_{abcN} is dropped, as shown in fig.3.8(c). The CE of the given system are deliberately selected as in fig.3.8(d). It can be seen that they have included all the necessary information for the set λ_{abc2N}.
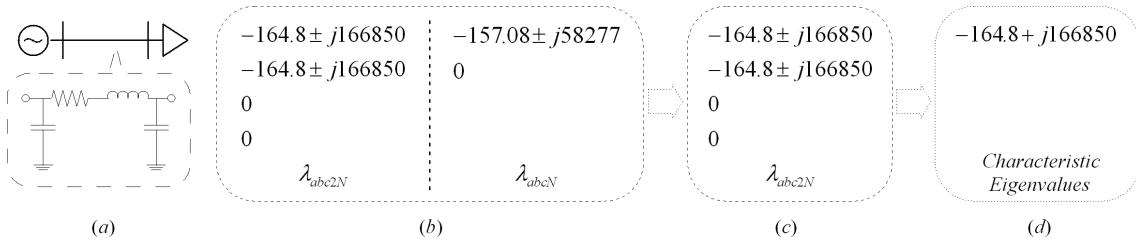
Figure 3.8: Explanation for the selection of characteristic eigenvalues

Compared to fig. 3.8(c), it can be noted that in fig. 3.8(d) the pair of zero eigenvalues is dropped. The reason is they have trivial meaning and their occurrence as well as the quantities can be expected by investigating the network topology. A further discussion is given as follows.

Observation

For a network, if its SN, EN and CN are all connected with an equivalent shunt capacitor, the set λ_{abc2N} will consist of two eigenvalues at the origin (the definitions of SN, EN and CN is in section 3.2).

Discussions

The explanation of the above observation is divided into two steps. Step 1 justifies that if the requirements are met, the system will have eigenvalues at the origin. Step 2 verifies

the quantity of the zero eigenvalues is 2.

- Step 1:

  The state space model of the network is given by $\dot{\mathbf{x}} = \mathbf{Ax} + \mathbf{Bu}$. From the analysis in section 3.2, it can be seen that SN, EN and CN are the interface of the network to other system components, such as generators, loads, etc. If every SN, EN and CN has an equivalent shunt capacitance, then in the state space model, the input vector $\mathbf{u}$ only consists of currents ($\mathbf{u} = [i_1 \ i_2 \ ... \ i_n]^T$). To simplify the discussion, all the currents are set to zero except i_1, i.e., $\mathbf{u} = [i_1 \ 0 \ ... \ 0]^T$ (here i_1 is a constant value). Under this assumption, since all the system nodes are either isolated from the ground or connected to the ground via a shunt capacitance, thus theoretically the constant current source i_1 will drive all the nodal voltages increasingly to infinity. This matches the observation that the network has eigenvalues at the origin.

  However, if some nodes of the SN, EN and CN do not have an equivalent shunt capacitance, then the input vector $\mathbf{u}$ will consist of both currents and voltages($\mathbf{u} = [i_1 \ ... \ v_i \ ... \ i_n]^T$). If still specifically chosen $\mathbf{u} = [i_1 \ 0 \ ... \ 0]^T$, this physically means node i has been directly grounded. Thus the constant current source i_1 will only result in a limited system response (for example, limited nodal voltages). Therefore there are no eigenvalues at the origin in this case.

- Step 2:

  To directly justify the quantity of the zero eigenvalues is difficult. Thus some examples are studied and the numerical results are reported instead.

  Fig. 3.9(a) gives a simple system, in which the network parameters are the same as those of appendix B. In fig. 3.9(b)-(e), symbols for generators and loads are omitted to make the plot clear. In fig. 3.9(a), all nodes do not have a shunt capacitance. On the contrary, all the SN, EN and CN in fig. 3.9(b) have a shunt capacitance. While in fig. 3.9(c)-(e), one of the SN, EN and CN does not have a shunt capacitance. The corresponding eigenvalue sets of λ_{abc2N} are reported in table 3.2. It can be seen that only in the case given in fig. 3.9(b), two eigenvalues appear at the origin.
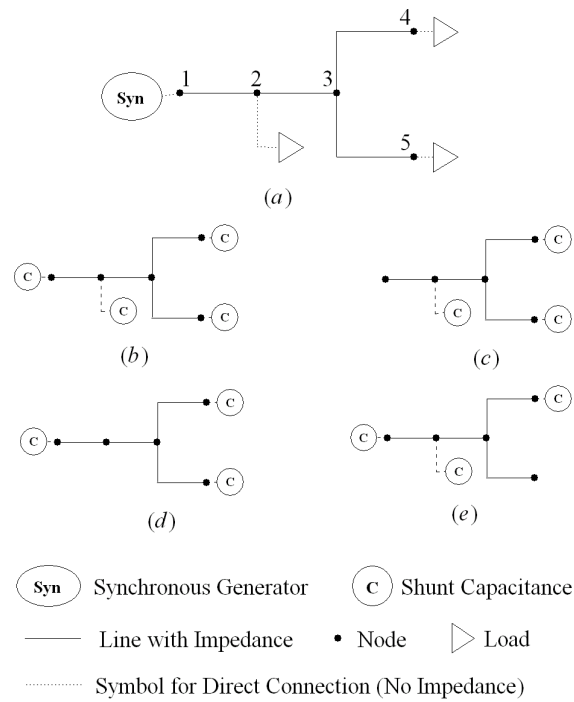
Figure 3.9: Examples for investigating the properties of the characteristic eigenvalues

Case of	λ_{abc2N}
fig.3.9(*a*)	-80.331, -80.331, -49.716, -49.716, -25.133, -25.133
fig.3.9(*b*)	$-37.667 \pm j8115.9$, $-37.667 \pm j8115.9$, $-24.764 \pm j6205$, $-24.764 \pm j6205$, $-15.159 \pm j16598$, $-15.159 \pm j16598$, 0, 0
fig.3.9(*c*)	$-34.048 \pm j7866.8$, $-34.048 \pm j7866.8$, $-23.51 \pm j3972.7$, $-23.51 \pm j3972.7$, $-20.032 \pm j13372$, $-20.032 \pm j13372$
fig.3.9(*d*)	$-36.927 \pm j7995.1$, $-36.927 \pm j7995.1$, $-28.096 \pm j4706.2$, $-28.096 \pm j4706.2$, $-12.566 \pm j11107$, $-12.566 \pm j11107$
fig.3.9(*e*)	$-37.762 \pm j7639.4$, $-37.762 \pm j7639.4$, $-24.64 \pm j3298.6$, $-24.64 \pm j3298.6$, $-15.188 \pm j16584$, $-15.188 \pm j16584$

Table 3.2: Eigenvalues of the systems given in fig. 3.9

Distributions of the Characteristic Eigenvalues of the Study Network I and Its Variants

The CE of the SNI are plotted in fig. 3.11(a). It is worth noting that all the CE of the network in fig. 3.6 have similar real parts though the imaginary parts vary considerably. Further, these real part values match those given in fig. 3.8(d). In order to get some more general conclusions about the distribution of the CE, more cases are studied, which are variants of the system in fig. 3.6. The variations include both the network topology and the line parameters.

The variant networks are shown in fig. 3.10, in which, the line between nodes 824 and 828 is removed, and a new line is added between nodes 826 and 834 in fig. 3.10(a) and between nodes 814 and 858 in fig. 3.10(b) respectively.
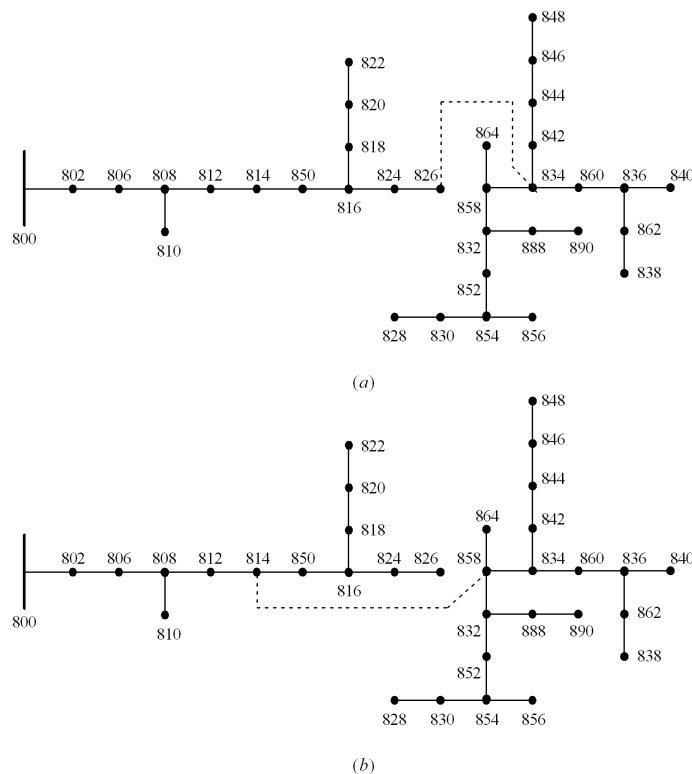
Figure 3.10: Variants of the SNI

The two topologies in fig. 3.10 will be referred to as 'T2' and 'T3', while the topology in fig. 3.6 will be referred to as 'T1'. For line parameters, the variations as well as the

original one can also be separated as three groups:

- For the first group (later referred to as 'P1'), the line parameters are given in appendix B. If the length of one of the lines is 1km, its CE is $-164.8 + j166850$, as given in fig. 3.8.

- For the second one (later referred to as 'P2'), the parameters of the lines 808-812, 816-824 and 860-836 are altered as: $R_n = 2 \times R$, $L_n = L/2$, $C_n = C$, where R, L, C have the same values given in appendix B, while R_n, L_n, C_n the altered parameters of the lines. If the length of one of the altered lines is 1km, its CE is $-659.22 + j235960$.

- For the third group (later referred to as 'P3'), besides the alteration of the lines 808-812, 816-824 and 860-836 as in the second group, lines 830-854, 854-856 and 854-852 are also changed as: $R_n = R/2$, $L_n = 2 \times L$, $C_n = C$. If the length of one of the altered lines is 1km, its CE is $-41.2 + j117980$.

Detailed information of each studied case is summarized in table 3.3.

Case No.	Network Topology	Line Parameters	Plot of Characteristic Eigenvalues
1	T1	P1	fig.3.11(a)
2	T2	P1	fig.3.11(b)
3	T3	P1	fig.3.11(c)
4	T1	P2	fig.3.11(d)
5	T2	P2	fig.3.11(e)
6	T3	P2	fig.3.11(f)
7	T1	P3	fig.3.11(g)
8	T2	P3	fig.3.11(h)
9	T3	P3	fig.3.11(i)

Table 3.3: Detailed information of the SNI and the variants

From fig. 3.11(a)-(c), it can be seen that though the network topology changes, the real parts of the CE remain unchanged, which match the one given in fig. 3.8(d). This indicates that, compared to network topology, line parameters predominantly determine the

real parts of the CE. This observation can be verified by investigating fig. 3.11(d)-(i). Using fig. 3.11(d)-(f) as an example, in which the distribution of the CE are similar though the differences among them are distinct; while the comparison of fig. 3.11(a)-(c) to fig. 3.11(d)-(f) seems to reveal that the CE are subjected to a large change. Hence, though the topology has an influence on the CE, the parameters of the line are of much greater influence.

A more instructive principle about the relation between the line parameters and the CE of the network can be formed as: assuming a network consists of M different types of lines, then the maximum and minimum values of the real parts of their CE span a range, which covers the real part values of the CE of the network. An explanation is given based on case 9. In it, the network has 3 different types of lines. The real parts of their CE are -41.2, -164.8 and -659.22 respectively. Their maximum and minimum values of the real parts span a range from -41.2 to -659.22, which totally covers the range spanned by the real parts of the CE of the given network, which from fig. 3.11(i) can be noted as from -44.9 to -526.2.
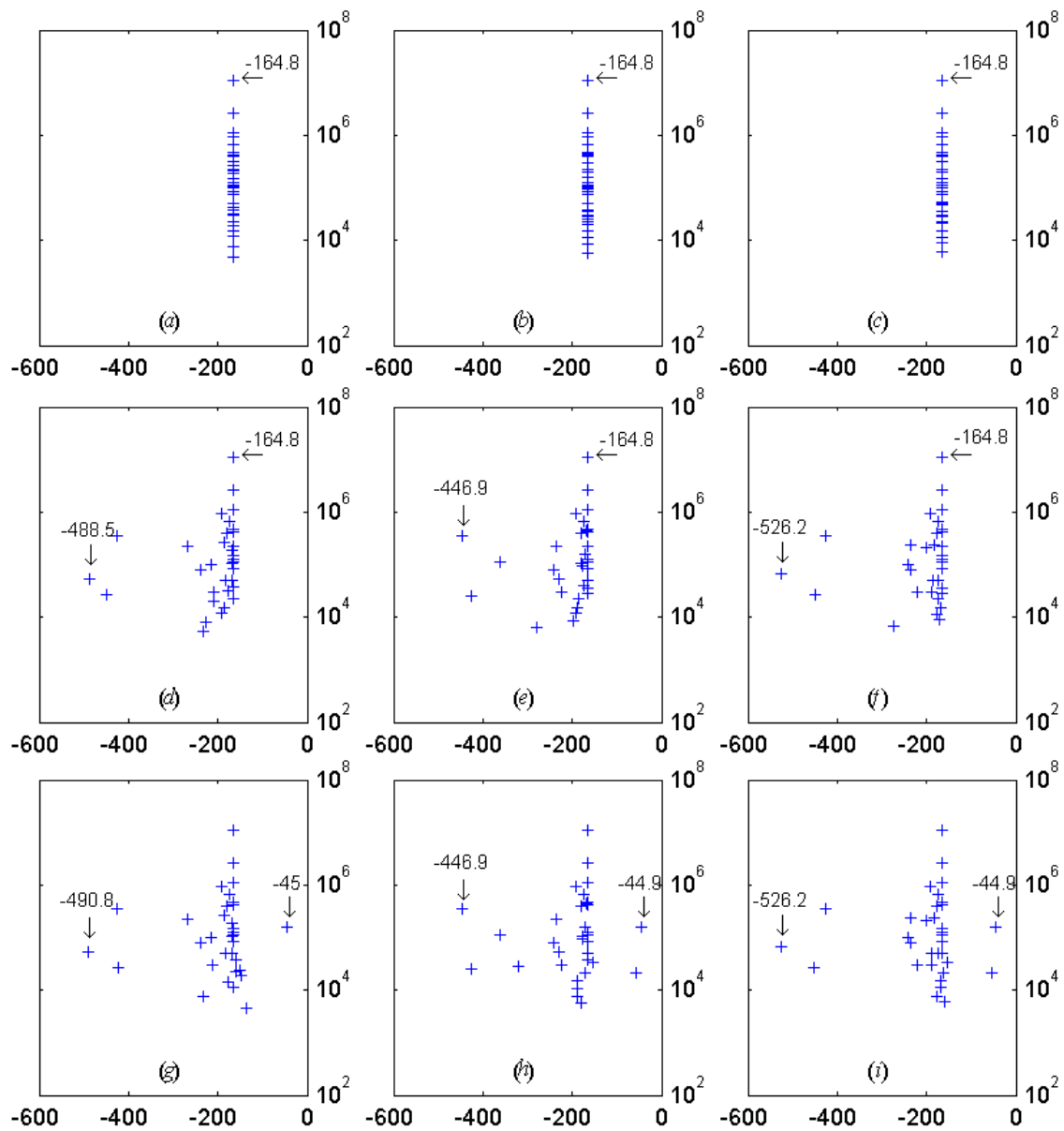
Figure 3.11: Distributions of the characteristic eigenvalues of the SNI and the variants

Distributions of the Characteristic Eigenvalues of the Study Network II

The CE of the SNII are plotted in fig. 3.12. Meanwhile, for ease of comparison, the CE of the cables used in the SNII are given in table 3.4.
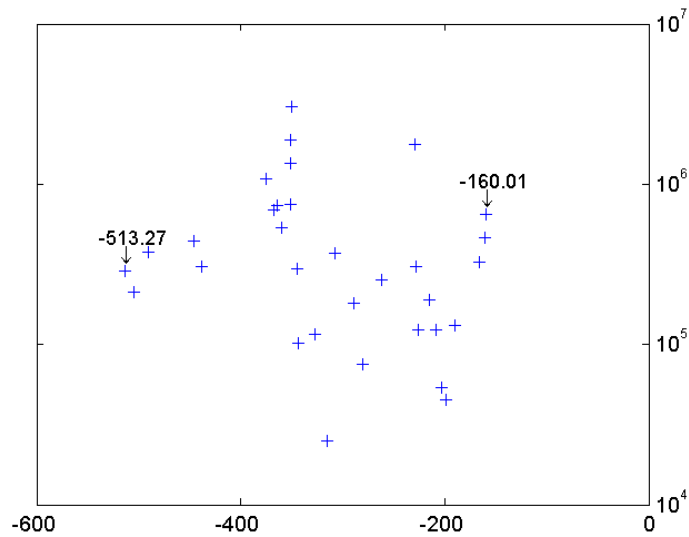
Figure 3.12: Distributions of the characteristic eigenvalues of the SNII

Type of cable	CE	Type of cable	CE
NA2XS(F)2Y $3\times1\times185$	-160.01 + j138820	NKBA 3×70	-409.31 + j191350
NAKBA 3×240	-229.44 + j161700	NAKBA 3×95	-507.37 + j184290
NAKBA 3×150	-350.92 + j172360	NAKBA 3×70	-673.63 + j191350

Table 3.4: Characteristic eigenvalues of the cables used in the SNII[†]

The results indicate that as for the cables of the SNII, the maximum and minimum values of the real parts of their CE span a range from -160.01 to -673.63, which totally covers the range spanned by the real parts of the CE of the SNII, which from fig. 3.12 can be noted as from -160.01 to -513.27. This conforms to the conclusions made in the previous part.

[†] When calculating the CE, all the cables are assumed to have a length of 1km.

3.4.2 Analysis of the Characteristics of Distribution Network Dynamics

Neplan [46] offers comprehensive information about the available lines/cables for the distribution systems with a voltage level from 1kV to 20kV in Europe. In its databank, the parameters of 361 types of lines/cables are given. These data are fully studied and the results reveal that, the maximum real part value of the CE of these lines/cables is -69.3, while the minimum value of that is -33055. Thus it can be expected that, the eigenvalues of a real distribution network in Europe will have real parts sited within the range from -69.3 to -33055. This means that a dynamic procedure caused by a certain disturbance will die down to 5% of its initial value within 0.0001s to 0.0433s. Though without proof of enough statistics, it is sensible to judge that normally the time intervals between two disturbances will be much bigger than 0.0433s. A bit work of clarifying the meaning of 'disturbance' used here may be helpful. In this thesis, the stochastic properties of DG are also deemed as kind of disturbances, though practically the alteration of its status may be the result of some normal operations, for example, the switching on/off of it.

From aforesaid analysis it can be seen that though apparently the disturbances are stochastic series, since the corresponding dynamic procedures last only quite a short period, the impact of each individual of the series to the electrical network is nearly independent. Besides, under this condition, it is still proper to adopt the steady state or quasi steady state assumptions to model the distribution network with DG.

3.4.3 Conclusions and Comments

This chapter focuses on studying the attributes of the electrical network dynamics of distribution systems. By investigating the eigenvalues of the state space model of the electrical network, the following conclusions are drawn:

- There is a close relation between the eigenvalues of the network under *abc* and *dq*0 reference frame. Assuming a symmetric network has $3N$ state variables, thus it has $3N$ eigenvalues. Among them, N pairs of the complex-conjugate/double-real eigenvalues under *abc* frame, relate only to the network *dq* components under *dq*0

frame. These eigenvalues under $dq0$ frame can be gotten by shifting the counterparts under abc frame with frequency of $\pm\omega_0$. The remaining N eigenvalues will keep unchanged under both of the two frames.

- The parameters of the lines/cables of the electrical network are the predominant factors to determine the eigenvalues of the network. Although the network topology has an influence on the eigenvalues, the parameters of the lines/cables are of much greater influence.

- The distribution of the eigenvalues of the network is bounded by the relevant values of its lines/cables. Assuming a distribution network consists of M different types of lines, then the maximum and minimum values of the real parts of their CE span a range, which covers the total interval spanned by the real parts of the CE of the network.

- In a real distribution network in Europe, the eigenvalues will have the real parts within the range from -69.3 to -33055. This is based on a thorough investigation of the data of the lines/cables given in Neplan [46].

- The impacts of the apparently successive stochastic disturbances to the network can be studied independently and the nodal admittance matrix is acceptable as the model of a distribution network. The investigation on the eigenvalues of a distribution network reveals that the electrical dynamics die off very fast. Hence a steady state assumption for modeling the distribution network is acceptable. The apparently successive stochastic disturbances have nearly independent influences on the network.

So far, some instructive conclusions are obtained. However, some limitations about the results exist as well. They are:

- The eigenvalues of set λ_{abcN} are not included in the discussion of section 3.4.1. However, it can be reasonably expected that the concerned conclusion is also applicable to λ_{abcN}. That is, assuming the network consists of M different types of lines, then the maximum and minimum values of the real parts of their CE in λ_{abcN} span

a range, which covers the total interval spanned by the real parts of the CE of the network in λ_{abcN}.

- Frequency dependence of line parameters is not considered when calculating the eigenvalues. Thus the results may not match the practical observations. A possibly improved approach is: 1. assuming the system is stepwise frequency independent; 2. forming the state matrix within this frequency band ([47]-[51] are some references for modeling frequency dependent lines); 3. calculating the eigenvalues, and those whose imaginary parts conform to the predetermined frequency band will belong to the set of the eigenvalues of the real system; 4. step 1 to 3 can be executed iteratively until all the eigenvalues have been found. During this procedure, it is important to note that as frequency keeps rising, the π equivalent model for lines/cables will not be proper even for distribution networks, in which the length of the line/cable normally is short. Under this situation, distributed parameter models can be adopted instead. However, the network dynamic order and thus the quantity of the eigenvalues will increase.

- All the examples and studied systems in this chapter are based on radial network topology. Thus it is open for further study if the introduced results are also applicable to meshed networks. However, a positive answer can be reasonably expected.

Chapter 4

Impacts of DG on the Small Signal Stability of Distribution Systems

Small signal stability concerns the ability of a system to maintain stability under small disturbances. Modal analysis, as a common tool to investigate the small signal stability, is adopted in this chapter to investigate the influence of DG on the small signal stability of distribution systems.

In this chapter, section 4.1 gives a brief view of the implementation of the small signal stability analysis in power systems. Section 4.2 presents the models for all the relevant system components. Section 4.3 contains simulations, results and comments.

The work of this chapter shows that the integration of DG will not lead to any small signal instability problem, even if the penetration level of DG is high. Besides, proper shunt reactive compensation, such as the use of STATCOM, improves the small signal stability of the system as well as the penetration level of DG.

4.1 Implementation of the Small Signal Analysis in Power Systems

4.1.1 Basic Concepts of Modal Analysis

For a power system, if the dynamics of the electrical network are also included into the small signal stability analysis, the whole system will be described by an ODE model. However, as discussed in chapter 3, since the dynamics of the electrical network die out very fast, these dynamics can be neglected which hence leads to the assumption that the electrical network is always in a steady state. Under this assumption, a DEA model of the whole system will be built instead of an ODE one.

Generally, a DAE model of a power system has the form as

$$
\begin{aligned}
\dot{\mathbf{x}} &= f(\mathbf{x}, \mathbf{v}, \mathbf{u}) \\
0 &= g(\mathbf{x}, \mathbf{v})
\end{aligned}
\tag{4.1}
$$

where
$\mathbf{x}$ is a vector of state variables;
$\mathbf{v}$ a vector of algebraic variables;
$\mathbf{u}$ a vector of disturbances or control inputs;
f represents the nonlinear dynamic characteristics of system components;
g the nonlinear relations between $\mathbf{x}$ and $\mathbf{v}$.

A linearized model around an operating point can be deduced from eqn. (4.1) as

$$
\begin{aligned}
\Delta\dot{\mathbf{x}} &= J_{fx}\Delta\mathbf{x} + J_{fv}\Delta\mathbf{v} + J_{fu}\Delta\mathbf{u} \\
0 &= J_{gx}\Delta\mathbf{x} + J_{gv}\Delta\mathbf{v}
\end{aligned}
\tag{4.2}
$$

where J_{fx}, J_{fv}, J_{fu}, J_{gx} and J_{gv} are the respective Jacobian matrices.

Eliminating the algebraic variables $\mathbf{v}$ in eqn. (4.2) leads to

$$
\Delta\dot{\mathbf{x}} = \mathbf{A}\Delta\mathbf{x} + \mathbf{B}\Delta\mathbf{u}
\tag{4.3}
$$

where $\mathbf{A} = J_{fx} - J_{fv}J_{gv}^{-1}J_{gx}$, $\mathbf{B} = J_{fu}$.

In eqn. (4.3), $\mathbf{A}$ is the state matrix. The small signal stability can be evaluated by investigating its eigenvalues.

Mode shape and eigenvectors [21]

Assuming $\mathbf{A}$ a $n \times n$ matrix, thus it has n eigenvalues:

$$\lambda = \lambda_1, \lambda_2, ... \lambda_n$$

For each eigenvalue λ_i, its associated n-column right eigenvector Φ_i satisfies the following equation:

$$\mathbf{A}\Phi_i = \lambda_i \Phi_i \tag{4.4}$$

Similarly, the so-called left eigenvector Ψ_i contains n rows and satisfies the equation:

$$\Psi_i \mathbf{A} = \lambda_i \Psi_i \tag{4.5}$$

Physically, the right eigenvector describes how each mode of oscillation is distributed among the systems states and it is called mode shape. The left eigenvector determines the combination of the state variables on a specific mode.

Participation matrix [21]

The participation matrix $\mathbf{P}$ combines the right and left eigenvectors to measure the relation between the state variables and the modes.

$$\mathbf{P} = [\mathbf{p}_1 \ \mathbf{p}_2 \ ... \ \mathbf{p}_n] \tag{4.6}$$

with

$$\mathbf{p}_i = \begin{bmatrix} p_{1i} \\ p_{2i} \\ ... \\ p_{ni} \end{bmatrix} = \begin{bmatrix} \phi_{1i}\psi_{i1} \\ \phi_{2i}\psi_{i2} \\ ... \\ \phi_{ni}\psi_{in} \end{bmatrix}$$

where

ϕ_{ki} is the element on the kth row and i^{th} column of the modal matrix Φ, with $\Phi = [\Phi_1 \ \Phi_2 \ ... \ \Phi_n]$;

ψ_{ik} is the element on the ith row and k^{th} column of the modal matrix Ψ, with $\Psi = [\Psi_1^T \ \Psi_2^T$
$\ldots \ \Psi_n^T \ ]^T$;

$p_{ki} = \phi_{ki}\psi_{ik}$ is the participation factor measuring the relative participation of the kth state
variable in the ith mode, and vice versa.

Damping ratio [21]

The damping ratio ξ determines the decaying rate of the amplitude of an oscillation. For
a complex-conjugate pair of eigenvalues

$$\lambda = \sigma \pm j\omega \tag{4.7}$$

the corresponding damping ratio is defined as

$$\xi = \frac{-\sigma}{\sqrt{\sigma^2 + \omega^2}} \tag{4.8}$$

4.1.2   Selection of a Common Reference Frame

In a multimachine system, it is normal to refer all the models to a CRF. The determination
of the CRF is presented in section 3.1.1.

4.1.3   Some Specifics of the Power System Model

The formulation of the state matrix of a power system involves steps of linearizing com-
ponent models and eliminating all the algebraic variables. Various components and their
large quantities make this procedure very complex. In order to form the state matrix **A** in
a systematic way, in this thesis the algebraic variables in eqn. (4.1) are specifically cho-
sen as the amplitude and argument of the nodal voltages, while the component models are
coupled with the network equations via the principle of power conservation. This means
that in eqn. (4.1), the nonlinear equations g can be rewritten as

$$0 = g_1(\mathbf{x}, \mathbf{v}) + g_2(\mathbf{v}) \tag{4.9}$$

where

g_1 describes the quantities of the power generated/consumed by system components, such
as generators, loads, FACTS devices, etc;

g_2 is the power transferred by the network, actually, which has the same form as in a

traditional power flow calculation.

The principle of the power conservation is reflected by the sum of g_1 and g_2 in eqn. (4.9) equal to zero.

4.2   Models of Power System Components

4.2.1   Equivalent of the Transmission System

In this thesis, since more attention is paid to the influence of DG on the distribution system, the transmission system is modeled by a synchronous generator with a large capacity. The classical model is adopted here for the reason that the impact of the operation status of the distribution system to the transmission system is not strong hence the equivalent synchronous generator need not to be modeled in detail. The corresponding mathematical model is

$$\begin{aligned}
\dot{\delta} &= \omega_0(\omega - 1) \\
\dot{\omega} &= (P_m - P_e - D(\omega - 1))/M
\end{aligned} \tag{4.10}$$

Where P_m is the mechanical power, P_e the electrical power, D the damping coefficient and M the inertia constant.

The electrical power P_e can be calculated as

$$P_e = (v_q + r_a i_q)i_q + (v_d + r_a i_d)i_d \tag{4.11}$$

Meanwhile, the relations between the voltages and the currents are

$$\begin{aligned}
0 &= v_q + r_a i_q - e'_q + x'_d i_d \\
0 &= v_d + r_a i_d - x'_d i_q
\end{aligned} \tag{4.12}$$

where e'_q is the q-axis transient voltage, r_a the stator resistance, and x'_d the d-axis transient reactance.

In eqn. (4.11) and (4.12), v_d and v_q are voltage components referred to the individual

$dq0$ frame of the synchronous generator. They are connected with the stator voltage under the CRF via

$$
\begin{aligned}
v_d &= V\sin(\delta - \theta_V) \\
v_q &= V\cos(\delta - \theta_V)
\end{aligned}
\tag{4.13}
$$

where V is the amplitude of the stator voltage, θ_V the angle referred to the CRF.

Similarly, i_d and i_q are current components referred to the individual $dq0$ frame of the synchronous generator. However, it is not necessary to formulate some equations similar to eqn. (4.13), to relate i_d and i_q to the stator current under the CRF, since they have already been connected to the algebraic variables v_d and v_q through eqn. (4.12).

The power injections from the generator are

$$
\begin{aligned}
P &= v_d i_d + v_q i_q \\
Q &= v_q i_d - v_d i_q
\end{aligned}
\tag{4.14}
$$

4.2.2   Network

As analyzed in chapter 3, since the dynamics of a distribution network die out very fast, when studying the small signal stability, it is proper to assume that the network is always in a steady state, or more accurately, a quasi steady state. Thus the corresponding mathematic model of the network is a nodal admittance matrix.

4.2.3   Constant Speed Wind Turbine Generation System

The DG in this chapter are specifically designated as constant speed wind turbine generation systems. The reason is that: compared to other DG technologies, the mathematically mature models of the wind generation systems (WGS) are available; further, among all the available WGS, the constant speed wind turbine generation system has the biggest interaction with the connected power system.

The model of the constant speed wind turbine generation system used in this work is presented in [31], which stems from the original one proposed in [4].

The Mechanical Power Extracted by Wind Turbine from the Wind

The mechanical power extracted by wind turbine from the wind can be calculated as

$$P_w = \frac{\rho}{2} c_p(\lambda) A_r v_w^3 \tag{4.15}$$

where, ρ is the air density, c_p the performance coefficient or power coefficient, A_r the area covered by the wind turbine rotor and λ the tip speed ratio (the ratio between the blade tip speed v_t(m/s) and the wind speed v_w(m/s) at the hub height upstream the rotor):

$$\lambda = \frac{v_t}{v_w} = \eta_{GB} \frac{2R\omega_{wr}}{p v_w} \tag{4.16}$$

with η_{GB} the gear box ratio, p the number of poles of the induction generator, R the rotor radius, and ω_{wr} the mechanical angular speed of the wind turbine.

Additionally, the following equation is used to approximate the c_p curve:

$$c_p = 0.44 \left(\frac{125}{\lambda_i} - 6.94 \right) e^{-\frac{16.5}{\lambda_i}} \tag{4.17}$$

with $\lambda_i = \frac{1}{\frac{1}{\lambda} + 0.002}$.

Shaft Model

A two mass representation has been adopted to describe the dynamic behavior of the mechanical driving subsystem which delivers the mechanical power from the rotor to the induction generator:

$$
\begin{aligned}
\dot{\omega}_{wr} &= \frac{T_{wr} - K_s \gamma}{2 H_{wr}} \\
\dot{\omega}_m &= \frac{K_s \gamma - T_e}{2 H_m} \\
\dot{\gamma} &= 2\pi f (\omega_{wr} - \omega_m)
\end{aligned}
\tag{4.18}
$$

where, f is the nominal grid frequency, γ the angular displacement between the two ends of the shaft, K_s the shaft stiffness, T_{wr} the torque, H_{wr} the inertia constant of the wind turbine, T_e and H_m the corresponding values of the generator, and ω_m the mechanical angular speed of the generator.

In equation (4.18), the mechanical torque T_{wr} and the electrical torque T_e are given by:

$$
\begin{aligned}
T_{wr} &= \frac{P_w}{\omega_{wr}} \\
T_e &= e'_r i_r + e'_m i_m
\end{aligned}
\tag{4.19}
$$

while the explanation of e'_r, i_r, e'_m and i_m is in the following paragraph.

Generator Model

The generator used in a constant speed generating system is a squirrel cage induction generator. Single cage representation for the rotor is adopted. When the stator transients are neglected, the model of the generator has the order of 2 and can be expressed as follows:

$$
\begin{aligned}
\dot{e}'_r &= \omega_0(1-\omega_m)e'_m - \frac{e'_r - (x_0 - x')i_m}{T'_0} \\
\dot{e}'_m &= -\omega_0(1-\omega_m)e'_r - \frac{e'_m + (x_0 - x')i_r}{T'_0}
\end{aligned}
\tag{4.20}
$$

with algebraic constraints as

$$
\begin{aligned}
e'_r - v_r &= r_s i_r - x' i_m \\
e'_m - v_m &= r_s i_m + x' i_r
\end{aligned}
\tag{4.21}
$$

where x_0, x' and T'_0 can be obtained from the generator parameters of rotator resistance r_R, rotator reactance x_R, stator reactance x_S and magnetizing reactance x_m as:

$$
\begin{aligned}
x_0 &= x_S + x_m \\
x' &= x_S + \frac{x_R x_m}{x_R + x_m} \\
T'_0 &= \frac{x_R x_m}{\omega_0 r_R}
\end{aligned}
\tag{4.22}
$$

and v_r, v_m, i_r and i_m are the projections of the stator voltage and current to the CRF.

The following relations between v_r, v_m and the stator voltage hold

$$
\begin{aligned}
v_r &= V\sin(-\theta_V) \\
v_m &= V\cos\theta_V
\end{aligned}
\tag{4.23}
$$

where V and θ_V are the amplitude and argument of the stator voltage in the CRF.

Electric Power Generated by the Wind Energy Conversion

The generated power is given by

$$
\begin{aligned}
P &= v_r i_r + v_m i_m \\
Q &= v_m i_r - v_r i_m + b_c(v_r^2 + v_m^2)
\end{aligned}
\tag{4.24}
$$

where b_c is the compensating capacitor conductance.

4.2.4   STATCOM

Based on the works in [52]-[57] and [7], an improved STATCOM model is developed and presented in this section.
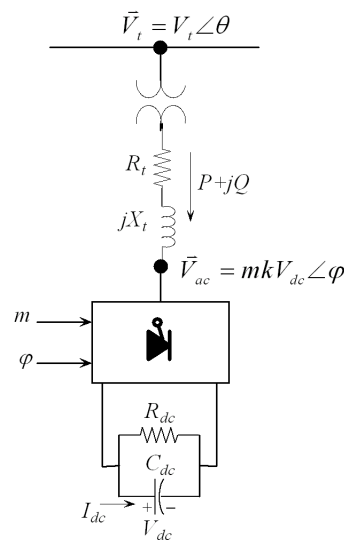
Figure 4.1: Electrical diagram of STATCOM

Pulse width modulation (PWM) is assumed to control the STATCOM via two principles: (1) by changing the ratio m to adjust the magnitude of the ac voltage and thus the exchange of the reactive power with the network; (2) by changing the phase angle φ between the network voltage and the voltage generated by the converter to feed the appropriate power from the network to balance the power loss of the STATCOM.

Before developing the STATCOM model, it is important to note that the per unit system adopted here is:

- for DC variables and AC variables in *abc* reference frame, the base voltage is the rated line-to-line voltage of the STATCOM.

- for variables in *dq*0 reference frame, the base voltage is the peak value of the rated line-to-neutral voltage of the STATCOM.

In both cases, the base power is the rated capacity of the STATCOM. Thus the following relations are valid:

$$
\begin{aligned}
S_b &= \sqrt{3}V_{abc}I_{abc} \\
Z_{abc} &= V_{abc}/\sqrt{3}I_{abc} \\
C_{abc} &= 1/\omega_0 Z_{abc}
\end{aligned}
\tag{4.25}
$$

and

$$
\begin{aligned}
S_b &= \frac{3}{2}V_{dq0}I_{dq0} \\
V_{abc} &= \sqrt{\frac{3}{2}}V_{dq0}
\end{aligned}
\tag{4.26}
$$

where, all the given values are the base quantities in the respective reference frames.

In fig. 4.1, the DC side dynamics satisfy

$$
\dot{V}_{dc} = \frac{I_{dc}}{C_{dc}}
\tag{4.27}
$$

Inserting eqn. (4.25) into eqn. (4.27) leads to the per unit model

$$
\dot{\bar{V}}_{dc} = \frac{\omega_0 \bar{I}_{dc}}{\sqrt{3}\bar{C}_{dc}}
\tag{4.28}
$$

where the superbar denotes the per unit variables.

Since the instant power at the AC and DC side must be equal, this results in

$$
V_{dc}I_{dc} + \frac{V_{dc}^2}{R_{dc}} = V_{aca}I_{aca} + V_{acb}I_{acb} + V_{acc}I_{acc}
\tag{4.29}
$$

where V_{aca} and I_{aca} are the AC voltage and AC current of phase *a* respectively, and so on.

Transforming eqn. (4.29) to *dq*0 frame and inserting eqn. (4.26) into it leads to

$$
\frac{1}{\sqrt{3}}\bar{V}_{dc}\bar{I}_{dc} + \frac{\bar{V}_{dc}^2}{\bar{R}_{dc}} = \bar{V}_{acd}\bar{I}_{acd} + \bar{V}_{acq}\bar{I}_{acq}
\tag{4.30}
$$

The AC voltage at the converter is

$$\bar{V}_{ac} = mk\bar{V}_{dc}\angle\varphi \qquad (4.31)$$

where m is the modulation ratio defined by PWM, k a ratio depending on the converter structure [58], in this work $k = \sqrt{\frac{3}{8}}$.

It is noted in advance that in the following equations, all the variables are expressed in per unit quantities. However, the superbar is omitted to make the equations concise.

Referring eqn. (4.31) to the CRF results in

$$
\begin{aligned}
V_{acd} &= mkV_{dc}\sin(-\varphi) \\
V_{acq} &= mkV_{dc}\cos\varphi
\end{aligned}
\qquad (4.32)
$$

Inserting eqn. (4.32) into eqn. (4.30) leads to

$$I_{dc} = \sqrt{3}mk(I_{acd}\sin(-\varphi) + I_{acq}\cos\varphi) - \frac{\sqrt{3}V_{dc}}{R_{dc}} \qquad (4.33)$$

Substituting eqn. (4.33) into eqn. (4.28) leads to

$$\dot{V}_{dc} = \frac{\omega_0}{C_{dc}}mk(I_{acd}\sin(-\varphi) + I_{acq}\cos\varphi) - \frac{\omega_0 V_{dc}}{R_{dc}C_{dc}} \qquad (4.34)$$

Assuming $\vec{I}_{ac} = I_{ac}\angle\theta_I$ (the superarrow denotes a phasor), this means

$$\vec{I}_{ac} = I_{ac}\cos\theta_I + jI_{ac}\sin\theta_I \qquad (4.35)$$

Referring $\vec{I}_{ac}$ to the CRF leads to

$$
\begin{aligned}
I_{acd} &= I_{ac}\sin(-\theta_I) \\
I_{acq} &= I_{ac}\cos\theta_I
\end{aligned}
\qquad (4.36)
$$

Combining eqn. (4.35) with (4.36) results in

$$
\begin{aligned}
I_{acd} &= -imag(\vec{I}_{ac}) \\
I_{acq} &= real(\vec{I}_{ac})
\end{aligned}
\qquad (4.37)
$$

Meanwhile, assuming $\vec{V_t} = V_t \angle \theta$ leads to

$$
\begin{aligned}
\vec{I}_{ac} &= \frac{\vec{V_t} - \vec{V}_{ac}}{Z_t} \\
&= (V_t \cos\theta - V_{ac}\cos\varphi)G_t - (V_t \sin\theta - V_{ac}\sin\varphi)B_t \\
&\quad + j((V_t \cos\theta - V_{ac}\cos\varphi)B_t + (V_t \sin\theta - V_{ac}\sin\varphi)G_t)
\end{aligned} \tag{4.38}
$$

Combining eqn. (4.37) with (4.38) leads to

$$
\begin{aligned}
I_{acd} &= -(V_t \cos\theta - V_{ac}\cos\varphi)B_t - (V_t \sin\theta - V_{ac}\sin\varphi)G_t \\
I_{acq} &= (V_t \cos\theta - V_{ac}\cos\varphi)G_t - (V_t \sin\theta - V_{ac}\sin\varphi)B_t
\end{aligned} \tag{4.39}
$$

Inserting (4.39) into (4.34) results in

$$
\dot{V}_{dc} = \frac{\omega_0}{C_{dc}}mk(V_t \sin(\varphi - \theta)B_t + (V_t \cos(\varphi - \theta) - mkV_{dc})G_t) - \frac{\omega_0 V_{dc}}{R_{dc}C_{dc}} \tag{4.40}
$$

In this work, two PI controllers shown in fig. 4.2 are adopted to control the m and φ in eqn. (4.31).
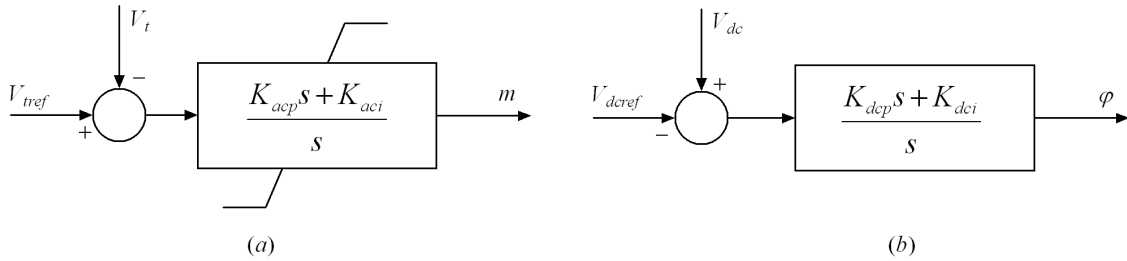
Figure 4.2: Controllers of STATCOM

It is worth noting that in fig. 4.2(b) the signs of V_{dcref} and V_{dc} are just opposite to those given in [53] and [54]. This can be explained with the help of fig. 4.3. Normally, V_{ac} lags behind V_t since the STATCOM will absorb active power from the network. This active power is used partly to compensate the STATCOM power losses and partly to charge the capacitor to increase its voltage. It is assumed that initially the STATCOM is under the steady state, thus V_{dc} equals V_{dcref}. Due to a disturbance, V_{dc} increases a bit. The difference between V_{dc} and V_{dcref} will generate a positive signal $\Delta\varphi$ which makes V_{ac} rotate counterclockwise a bit (from V_{ac} to V'_{ac}), thus decreases the angle gap between V_t and V_{ac}. This will reduce the active power fed by the network to the STATCOM, and consequently

decrease the voltage V_{dc}. Similarly, when a disturbance makes V_{dc} decrease a bit, analysis shows that the controller will try to make an increment of it. This indicates that the design in fig. 4.2(*b*) is stable.
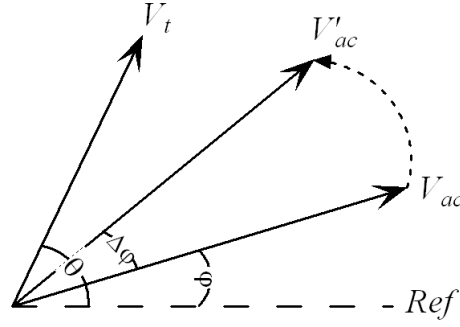
Figure 4.3: Explanation of the structure of the DC voltage controller in fig. 4.2

In the following the mathematical models of the STATCOM controllers are developed.

The AC voltage controller in fig. 4.2(*a*) is defined by

$$m = \frac{K_{acp}s + K_{aci}}{s}(V_{tref} - V_t) \tag{4.41}$$

Introducing

$$x_1 = \frac{1}{s}(V_{tref} - V_t)$$

leads to the time domain representation

$$\begin{aligned} \dot{x}_1 &= V_{tref} - V_t \\ m &= K_{acp}(V_{tref} - V_t) + K_{aci}x_1 \end{aligned} \tag{4.42}$$

The DC voltage controller in fig. 4.2(*b*) is given by

$$\varphi = \frac{K_{dcp}s + K_{dci}}{s}(-V_{dcref} + V_{dc}) \tag{4.43}$$

Introducing

$$x_2 = \frac{1}{s}(-V_{dcref} + V_{dc})$$

leads to

$$\dot{x}_2 = -V_{dcref} + V_{dc}$$

$$\varphi = K_{dcp}(-V_{dcref} + V_{dc}) + K_{dci}x_2 \qquad (4.44)$$

The power absorbed by the STATCOM from the network is given by

$$P = V_t^2 G_t - mkV_t V_{dc} G_t \cos(\theta - \varphi) - mkV_t V_{dc} B_t \sin(\theta - \varphi)$$

$$Q = -V_t^2 B_t + mkV_t V_{dc} B_t \cos(\theta - \varphi) - mkV_t V_{dc} G_t \sin(\theta - \varphi) \qquad (4.45)$$

Eqn. (4.40), (4.42), (4.44) and (4.45) constitute the complete model of the STATCOM.

In order to include the developed model of the STATCOM into the modal analysis, a linearization of the model is necessary.

The linearized model can be written as

$$\Delta \dot{\mathbf{x}} = J_{fx}\Delta \mathbf{x} + J_{fv}\Delta \mathbf{v} + J_{fu}\Delta \mathbf{u}$$

$$\Delta g_1 = J_{g_1x}\Delta \mathbf{x} + J_{g_1v}\Delta \mathbf{v}$$

where $\mathbf{x}$ is the state variable vector, which includes $[V_{dc}, x_1, x_2]^T$
$\mathbf{v}$ the algebraic variable vector, $\mathbf{v} = [\theta, V_t]^T$
$\mathbf{u}$ the input variable vector.

The Jacobian matrices are defined as

$$J_{fx}(1,1) = -\frac{\omega_0}{C_{dc}}m^2 k^2 G_t - \frac{\omega_0}{R_{dc}C_{dc}} + (\frac{\omega_0}{C_{dc}}mkV_t \cos(\varphi - \theta)B_t - \frac{\omega_0}{C_{dc}}mkV_t \sin(\varphi - \theta)G_t) * K_{dcp}$$

$$J_{fx}(1,2) = (\frac{\omega_0}{C_{dc}}kV_t \sin(\varphi - \theta)B_t + \frac{\omega_0}{C_{dc}}kV_t \cos(\varphi - \theta)G_t - 2\frac{\omega_0}{C_{dc}}mk^2 V_{dc}G_t) * K_{aci}$$

$$J_{fx}(1,3) = (\frac{\omega_0}{C_{dc}}mkV_t \cos(\varphi - \theta)B_t - \frac{\omega_0}{C_{dc}}mkV_t \sin(\varphi - \theta)G_t) * K_{dci}$$

$$J_{fx}(3,1) = 1$$

$$J_{fv}(1,1) = -\frac{\omega_0}{C_{dc}}mkV_t\cos(\varphi-\theta)B_t + \frac{\omega_0}{C_{dc}}mkV_t\sin(\varphi-\theta)G_t$$

$$J_{fv}(1,2) = \frac{\omega_0}{C_{dc}}mk\sin(\varphi-\theta)B_t + \frac{\omega_0}{C_{dc}}mk\cos(\varphi-\theta)G_t + $$
$$-(\frac{\omega_0}{C_{dc}}kV_t\sin(\varphi-\theta)B_t + \frac{\omega_0}{C_{dc}}kV_t\cos(\varphi-\theta)G_t - 2\frac{\omega_0}{C_{dc}}mk^2V_{dc}G_t)*K_{acp}$$

$$J_{fv}(2,2) = -1$$

$$J_{g_1x}(1,1) = -mkV_tG_t\cos(\theta-\varphi) - mkV_tB_t\sin(\theta-\varphi) + $$
$$(-mkV_tV_{dc}G_t\sin(\theta-\varphi) + mkV_tV_{dc}B_t\cos(\theta-\varphi))*K_{dcp}$$

$$J_{g_1x}(1,2) = (-kV_tV_{dc}G_t\cos(\theta-\varphi) - kV_tV_{dc}B_t\sin(\theta-\varphi))*K_{aci}$$

$$J_{g_1x}(1,3) = (-mkV_tV_{dc}G_t\sin(\theta-\varphi) + mkV_tV_{dc}B_t\cos(\theta-\varphi))*K_{dci}$$

$$J_{g_1x}(2,1) = mkV_tB_t\cos(\theta-\varphi) - mkV_tG_t\sin(\theta-\varphi) + $$
$$(mkV_tV_{dc}B_t\sin(\theta-\varphi) + mkV_tV_{dc}G_t\cos(\theta-\varphi))*K_{dcp}$$

$$J_{g_1x}(2,2) = (kV_tV_{dc}B_t\cos(\theta-\varphi) - kV_tV_{dc}G_t\sin(\theta-\varphi))*K_{aci}$$

$$J_{g_1x}(2,3) = (mkV_tV_{dc}B_t\sin(\theta-\varphi) + mkV_tV_{dc}G_t\cos(\theta-\varphi))*K_{dci}$$

$$J_{g_1v}(1,1) = mkV_tV_{dc}G_t\sin(\theta-\varphi) - mkV_tV_{dc}B_t\cos(\theta-\varphi)$$

$$J_{g_1v}(1,2) = 2V_tG_t - mkV_{dc}G_t\cos(\theta-\varphi) - mkV_{dc}B_t\sin(\theta-\varphi) + $$
$$(kV_tV_{dc}G_t\cos(\theta-\varphi) + kV_tV_{dc}B_t\sin(\theta-\varphi))*K_{acp}$$

$$J_{g_1v}(2,1) = -mkV_tV_{dc}B_t\sin(\theta-\varphi) - mkV_tV_{dc}G_t\cos(\theta-\varphi)$$

$$J_{g_1v}(2,2) = -2V_tB_t + mkV_{dc}B_t\cos(\theta-\varphi) - mkV_{dc}G_t\sin(\theta-\varphi) + $$
$$-(kV_tV_{dc}B_t\cos(\theta-\varphi) - kV_tV_{dc}G_t\sin(\theta-\varphi))*K_{acp}$$

4.2.5   Loads

The static load model is adopted here as to represent the active power as constant current component and the reactive power as constant impedance component.

4.3   Simulations and Results

4.3.1   Impacts of WGS on the Small Signal Stability of the SNI

When investigating the impact of WGS on the small signal stability of the SNI, the following factors are expected to have a relatively large influence on the results:

- *Load Level* —- A high load level is selected as corresponding to the load values in appendix B; while a low load level corresponds to 20% of the demand of the high load level.

- *Characteristics of the Connection of the Distribution System to the Transmission System* —- A strong connection is selected as corresponding to the line segment at 800-802 in fig. 3.6 with the specified length as in appendix B; while a week connection is obtained by stretching this line 10 times longer to 7.864 km.

- *WGS penetration level* —- Though there are no practical evidences, it can be reasonable to expect that the more WGS connected to the network, the higher their influences on the system operation. Thus it is assumed the WGS achieves its maximum allowable penetration level.

- *WGS generation level* —- The generation level is mainly determined by the wind speed, which in this work varies discretely from 0.4 p.u. to 1.0 p.u. rated wind speed (approximately corresponding to no generation to full generation) with a step of 0.1 p.u..

All the scenarios are classified into 4 groups according to the combinations of the above mentioned factors. Details are given in table 4.1.

	Group 1	Group 2	Group 3	Group 4
load level	high	low	high	low
connection characteristic of distribution to transmission systems	strong		weak	
WGS penetration level	maximum			
WGS generation level	stepwise changing from no to full generation			

Table 4.1: Detailed information of the studied scenarios

Determination of the Maximum Allowable Penetration Level of WGS

In this work, the maximum allowable penetration level of WGS is evaluated by the maximum number of WGS allowed to connect to the distribution network, which means that

for a given distribution system, if the maximum allowable number of WGS is n, then for all the possible scenarios, the system must be in a normal operation state; however, if there are totally $n+1$ WGS integrated to the network, then for some scenarios the system will be subjected to abnormal operation problems, which can be a steady state voltage violation, or a small signal instability problem, etc.

The penetration level is preliminarily determined by considering the fact that the steady state voltage of the network must stay within a fixed predetermined range. Here the allowable steady state voltage variation is adopted equal to $\pm10\%$ (0.9/1.1 p.u.). Later, the feasibility of the obtained penetration level will be verified by checking the status of the small signal stability.

In the following parts, the simulation procedures and results for the scenarios of group 1 and 2 are given in detail. At the end of this section, a brief view of the results for the scenarios of group 3 and 4 are available.

The maximum allowable numbers of the WGS connected to each node for group 1 and 2 are determined with the help of power flow computations. The results reveal that, the higher the generation level of the WGS, the lower the allowable penetration level of the WGS.

Fig. 4.4(*a*) and 4.4(*b*) present the results for the scenarios of group 1 and 2 respectively. To make the figures clear, only the results with the assumption that all the WGS are at the full power generation are shown.

From fig. 4.4 it can be seen when the WGS is connected to different nodes, the maximum allowable numbers of it vary quite a lot. It is worth emphasizing again, that these results are obtained according to the criterion of the nodal steady state voltage.

As stated in table 4.1, when investigating the small signal stability, the integration of the WGS is assumed to achieve the maximum level. In order to determine the specific number of the integrated WGS by referring to the results given in fig. 4.4, the following
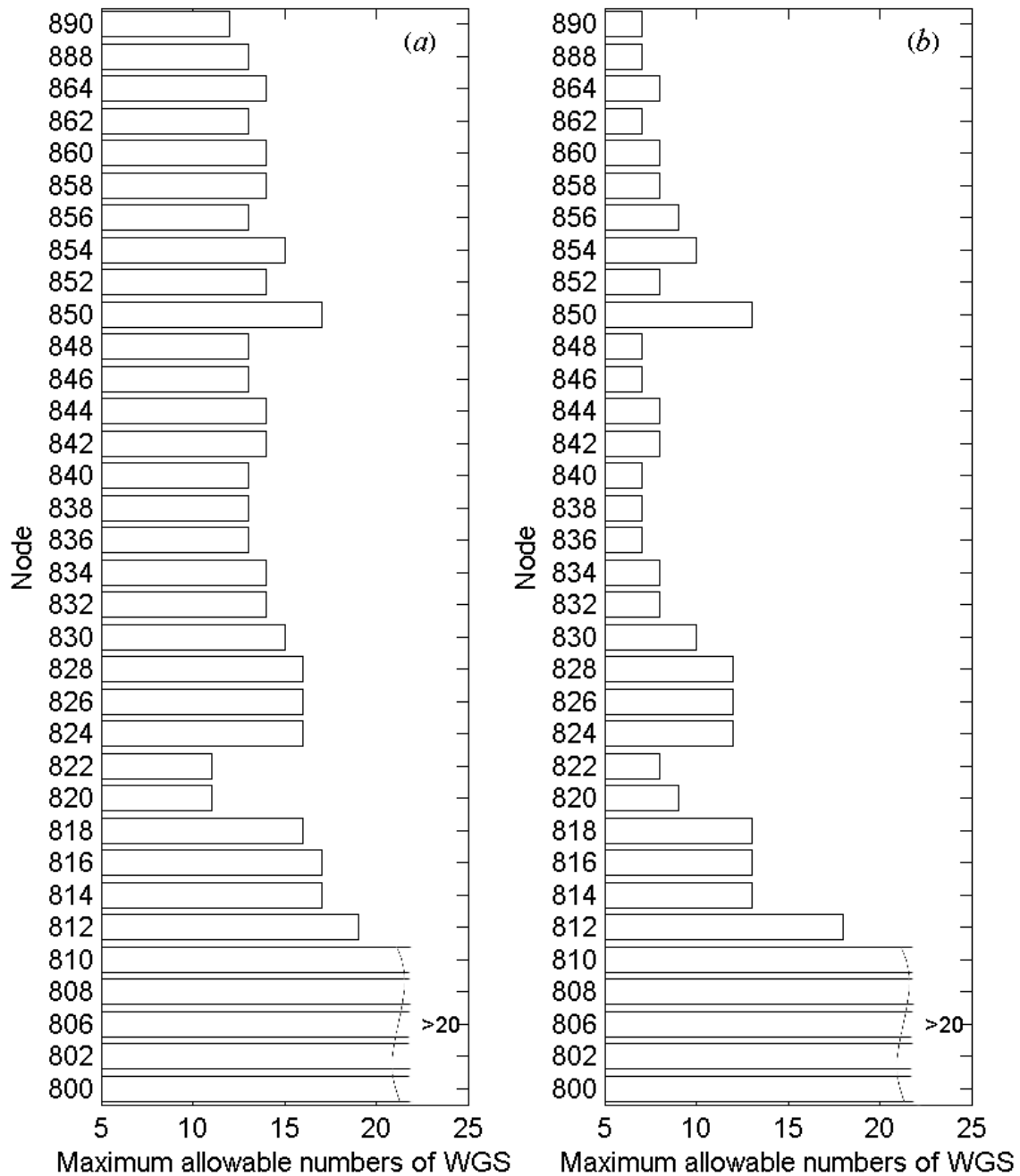
Figure 4.4: The maximum allowable numbers of the WGS connected to each node for group 1 and 2

considerations are relevant:

- In this thesis, since the objective is to evaluate the impacts of the DG rather than only the WGS on system operations in a more general sense, hence the WGS is assumed to be allowed to connect to the network arbitrarily, which may give a more suitable approximation to the potential operation of the DG in the future thus lead to a more general conclusion. This assumption implicitly puts forward a requirement as, to determine the number of the WGS from the presently available results given in fig. 4.4, it must be note that under all the possible distributions of the WGS, the steady state voltage must be in the fixed range. This requirement can be met by choosing the number of the WGS as the minimum one given in the figure, which for fig. 4.4(a) is 11, for fig. 4.4(b) is 7.

- Scenarios of group 1 and 2 should have the same maximum allowable penetration level of WGS, since they are based on a physically identical network.

The above considerations result in the conclusion that for the scenarios of group 1 and 2, the maximum number of WGS allowed to connect to the network is 7.

Impacts of WGS on the Small Signal Stability

As above mentioned, for the scenarios of group 1 and 2 the studied network allows at most 7 WGS to be connected. Before moving forward to deeper analyses, a general view about the possible distribution of the eigenvalues of the studied system may be helpful.

Table 4.2 gives a sample of the eigenvalues of the system with conditions as: the 7 WGS are connected to node 838; the wind blowing on them has speed as 0.4, 0.5, 0.6, 0.7, 0.8, 0.9 and 1.0 respectively.

A sensible model of wind speed for different WGS will consider the correlation among them. This is necessary when the long term system operations with WGS are investigated. However, this work focuses on studying the small signal stability at some certain moments, at which the system status is got by snapshooting the practical system state. Under this condition, the simplification as assuming the wind speeds at different spots are

independent, as adopted in the above discussion, is acceptable.

No.	Eigenvalue	Damping Ratio (%)	No.	Eigenvalue	Damping Ratio (%)
1	-17.222	100	17, 18	$-8.415 \pm j43.412$	19.03
2	-17.342	100	19, 20	$-8.438 \pm j43.405$	19.083
3	-17.478	100	21, 22	$-3.918 \pm j33.325$	11.677
4	-17.604	100	23, 24	$-0.462 \pm j4.232$	10.845
5	-17.746	100	25, 26	$-0.458 \pm j4.232$	10.767
6	-17.696	100	27, 28	$-0.449 \pm j4.228$	10.563
7	-10.771	100	29, 30	$-0.428 \pm j4.224$	10.074
8	-0.789	100	31, 32	$-0.395 \pm j4.218$	9.327
9, 10	$-8.653 \pm j43.129$	19.67	33, 34	$-0.354 \pm j4.209$	8.387
11, 12	$-8.600 \pm j43.205$	19.523	35, 36	$-0.311 \pm j4.196$	7.398
13, 14	$-8.540 \pm j43.29$	19.354	37	0	-
15, 16	$-8.482 \pm j43.362$	19.198			

Table 4.2: A sample of the eigenvalues for a specific scenario

As shown in table 4.2, when 7 WGS are connected to the studied network, the whole system totally has 37 eigenvalues. In them, the zero eigenvalue numbered 37 appears just due to the lack of uniqueness of absolute rotor angle [21], thus requires no further attention. However, it can be seen that the pair of eigenvalues numbered 35 and 36, have the minimum absolute values of the real part as well as the minimum damping ratio. Thus they may play a dominant role in the dynamic responses of the system. Therefore the impacts of WGS on the small signal stability can be investigated by studying the evolution of this pair of eigenvalues when other conditions, such as the locations, the generation levels of the WGS are changed. For ease of later reference, this pair of eigenvalues is named as 'Critical Eigenvalues' (CRE).

To investigate the influences of the integrated WGS on the small signal stability, factors as the locations and the generation levels of the WGS are expected to be most relevant. The total number of the possible scenarios makes an exhaustive study quite hard if not

impossible. Thus another analysis procedure consisting of three steps is proposed as follows:

- Firstly, evolutionary algorithm is used to form a conjecture about the relation between the concerned factors and the small signal stability.

- Then, the obtained conjecture is exploited as a direction for seeking the potentially worst scenario.

- Finally, lots of randomly generated scenarios are analyzed to verify the results. When the correctness of the results is justified, some general conclusions are drawn from them.

The details of the procedure are:

Step 1, applying evolutionary algorithm to identify the causality between the concerned factors and the potential problems of the small signal instability.

Evolutionary algorithm [59]-[64] has been successfully used for power system optimizations in many aspects. Since the interest of this work is to identify if a high penetration level of DG will induce the problems of the small signal instability, to find the potential scenario of which the CRE have the minimum damping ratio (compared to the damping ratio of the CRE of other scenarios), thus will be meaningful and important. The seeking of such a scenario can be proposed as a optimization problem, i.e., to find a combination of the concerned factors to achieve the minimum damping ratio of the CRE. Thus evolutionary algorithm is applicable in this case.

The structure of the evolutionary algorithm used in this work is shown in fig. 4.5.

The details of the implementation of the algorithm are as follows:

- In the stage of initialization, the population is set to have 50 individuals. Since there are 7 WGS under the consideration, further, for each WGS the location and the generation level are variables to be determined, thus each individual is coded to include 14 units, in which, the first 7 successive units indicate the locations of the
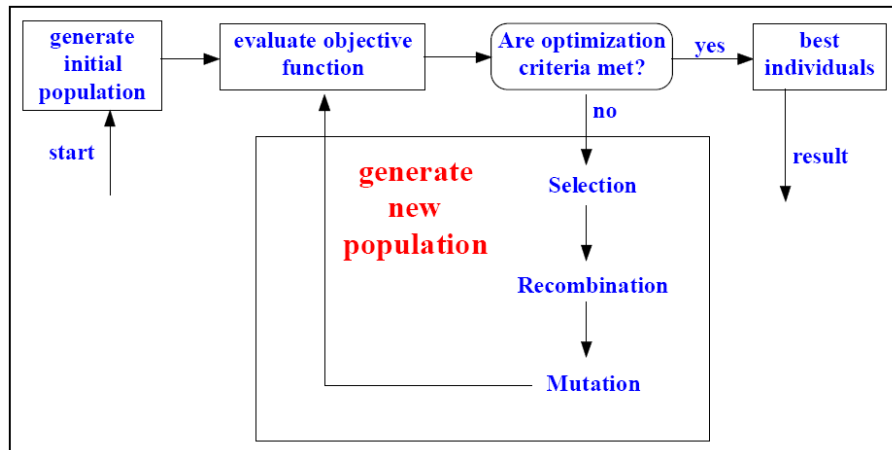
Figure 4.5: Structure of the evolutionary algorithm [65]

WGS, while the last 7 successive units record the wind speed. A schematic of such an individual is given in fig. 4.6.
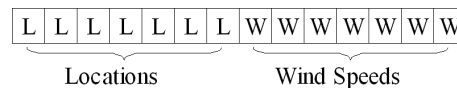
Figure 4.6: Schematic of a individual

- The objective function is to get the minimum value of the damping ratio of the CRE under all calculated scenarios.

- The optimization criteria, which serves actually as a convergence condition, is specifically chosen as the maximum generation number under which the value of the objective function keeps unchanged is more than 100.

- The fitness for the stage of selection is calculated through the following function

$$f_i = (\frac{1}{10 \times DR_i})^2 \tag{4.46}$$

where f_i is the fitness of the ith individual, DR_i the damping ratio of the CRE of the ith individual.

Besides, roulette-wheel selection is adopted as the selection scheme.

- The possibility of recombination is 0.5.

- The possibility of mutation is 0.2.

Fig.4.7(a) and (b) present the evolutions of the minimum damping ratio of the CRE for each generation of scenario groups 1 and 2. These figures can serve as an illustration of the convergence trajectories during the computation as well.
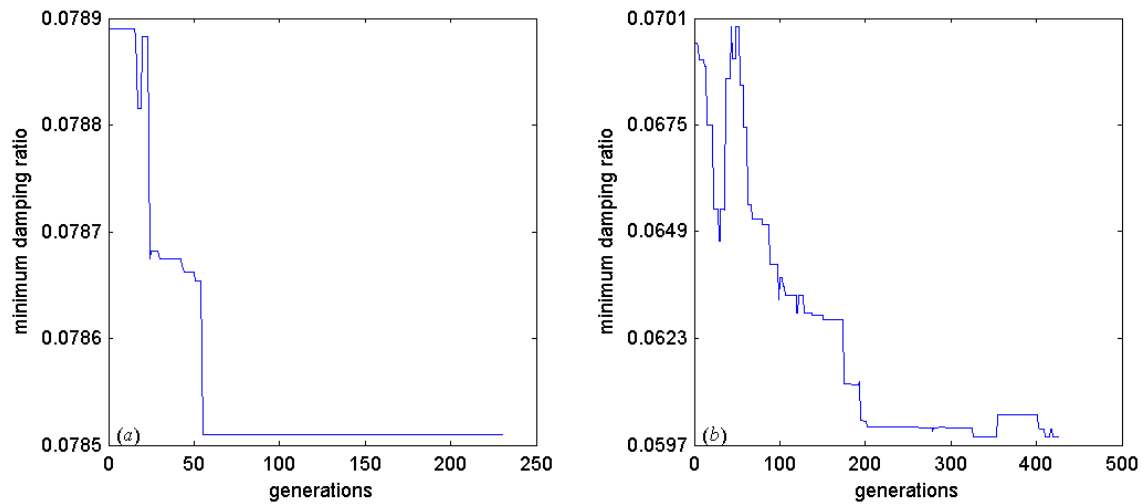
Figure 4.7: Convergence of the evolution

As shown in fig. 4.7, the evolutionary algorithms applied to the scenarios of group 1 and 2 converge after 230 and 426 generations respectively. The individuals which have the best fitness are reported as follows:

- For scenario group 1,

  the best individual:

800	812	848	844	828	862	800	1	1	0.7	1	0.8	1	1

  the damping ratio of the CRE: 0.0785

  the corresponding CRE: $-0.331 \pm j4.209$

- For scenario group 2,

  the best individual:

838	840	838	840	836	838	846	1	1	1	1	1	1	1

  the damping ratio of the CRE: 0.0599

  the corresponding CRE: $-0.251 \pm j4.175$

From the results it can be expected that the worst scenario appears when:

1. the WGS are connected to the nodes, which have a relatively weak connection to the network (normally these nodes will have a relatively big value of short circuit impedance);

2. the WGS have high generation levels.

These conjectures serve as a direction for the study in the following step.

Step 2, choosing nodes 822, 838, 840, 848, 856, 864 and 890 for a thorough study to seek the worst case. The reason of choosing these nodes is their relatively weak connections to the network. Further, the possible values of the wind speed are confined to 0.9 and 1.0, to give a high generation level.
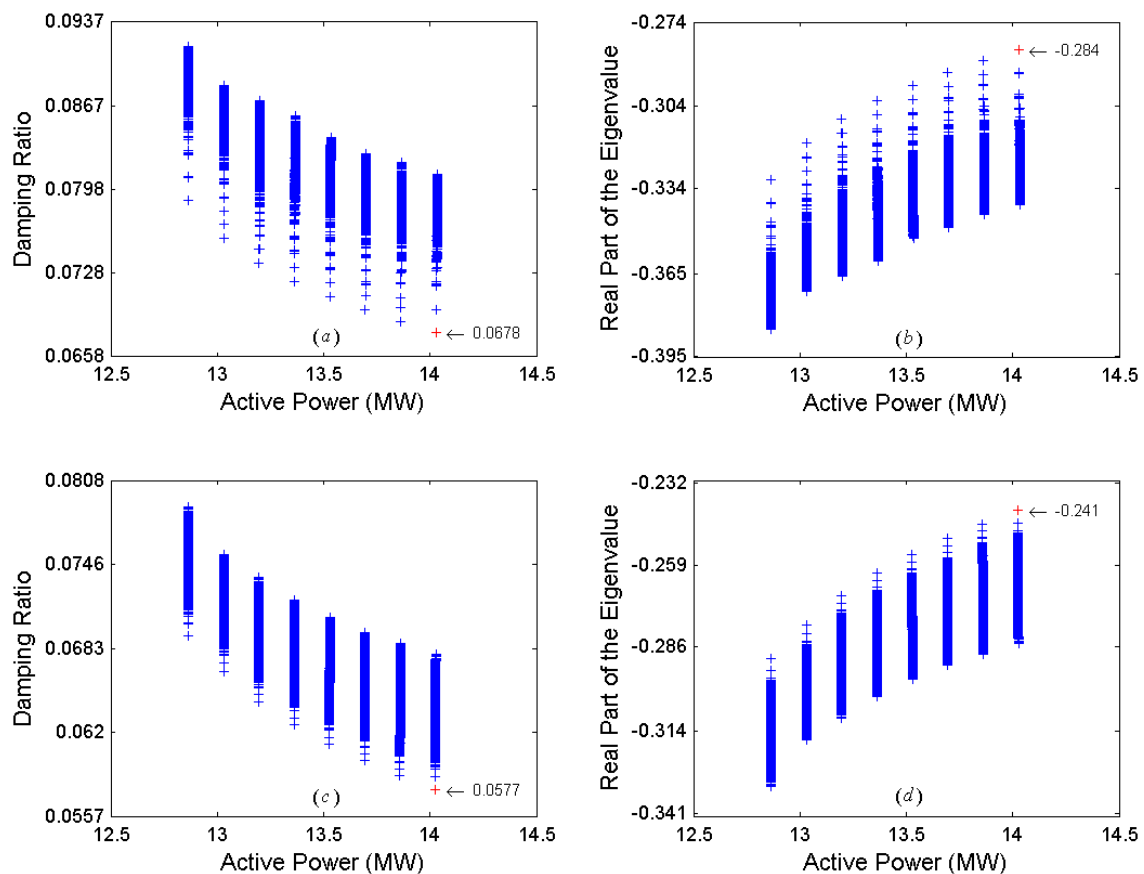
Figure 4.8: Determination of the worst scenario

Fig. 4.8(*a*) gives the relation of the sum of the active power of 7 WGS versus the damping ratios of the CRE for scenario group 1. In fig. 4.8(*b*) the relation between the generation

level of WGS and the real parts of the CRE is shown. Fig.4.8(*c*) and (*d*) report the corresponding results for scenario group 2.

Detailed information about the worst scenario is given as follows, in which, to make the expressions concise, the genetic structure used in the previous step is adopted:

- For scenario group 1,

  the conditions for the worst scenario:

822	822	822	822	822	822	822	1	1	1	1	1	1	1

  the damping ratio of the CRE: 0.0678

  the corresponding CRE: -0.284 $\pm$ j4.175

- For scenario group 2,

  the conditions for the worst scenario:

890	890	890	890	890	890	890	1	1	1	1	1	1	1

  the damping ratio of the CRE: 0.0577

  the corresponding CRE: -0.241 $\pm$ j4.171

By investigating the results, the conclusions made in the previous step for the occurrence of the worst scenario can be improved as follows

1. all the WGS are connected to a certain node which is a weak connection point of the network; however, this specific node varies when the operation status of the system, such as the load level, alters;

2. the WGS are with full power generation;

3. generally when the network is lightly loaded, the situation is worse.

These results are verified in the following step.

Step 3, computing a large amount of randomly generated scenarios to verify the results given above. In this step, for each scenario group of 1 and 2, 50000 scenarios are randomly generated. Their minimum damping ratios and the corresponding generation levels are reported in fig. 4.9(*a*) and (*b*) respectively. For convenience of the comparison, the worst case obtained in step 1 and 2 are also marked in it respectively with the symbols of $\square$ and $\triangle$.
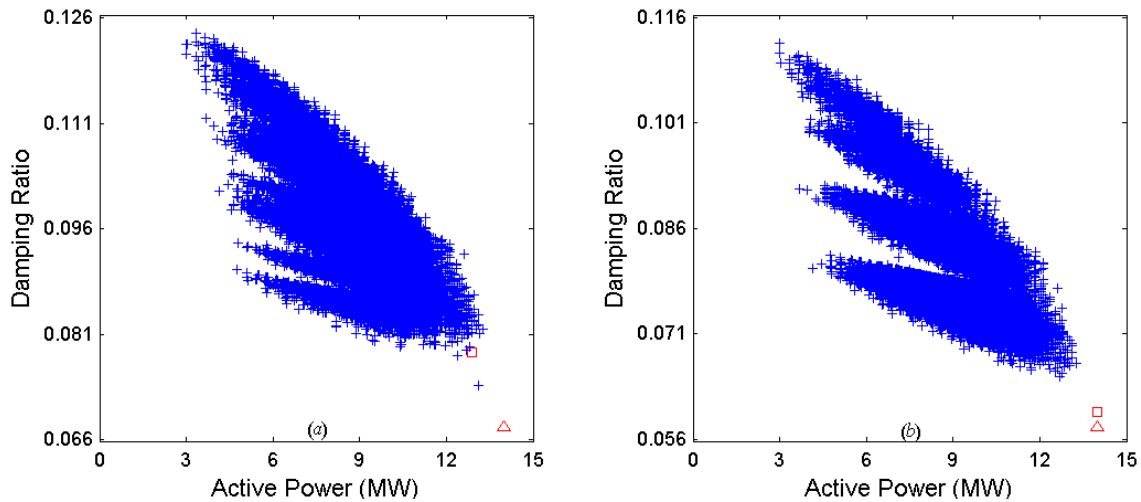
Figure 4.9: Result verification by a large amount of random scenarios

By considering the results obtained in step 1, 2 and 3, simultaneously observing the logical relationship among them, it is reasonable to conclude that step 2 figures out the worst scenario among all the potential candidates.

In [22], it is pointed out that for power systems, the minimum acceptable damping ratio should be not less than 0.03. This conclusion is summarized mainly based on the experience of transmission system operations. The application of it to distribution systems may need further verification. However, before more experiences and proper conclusions are available, it is meaningful to take it as a reference. With the help of it, a statement can be generalized as:

Normally the high penetration level of DG will not lead to small signal instability problems in distribution systems. Compared to the small signal stability, the steady state voltage rise of the system is a more important factor to determine the penetration level of DG.

Simulation Results for the Scenarios of Group 3 and 4

Studies on the scenarios of group 3 and 4 given in table 4.1 have been carried on with a same routine as that for group 1 and 2. Summaries of the results are given as follows:

- The maximum number of the WGS allowed to connect to the network is 6.

- For scenario group 3,

  the conditions for the worst scenario:

822	822	822	822	822	822	1	1	1	1	1	1

  the damping ratio of the CRE: 0.0718

  the corresponding CRE: -0.3 $\pm$ j4.166

- For scenario group 4,

  the conditions for the worst scenario:

890	890	890	890	890	890	1	1	1	1	1	1

  the damping ratio of the CRE: 0.0585

  the corresponding CRE: -0.245 $\pm$ j4.170

Comparing these results to those of scenario group 1 and 2 leads to conclusions as:

- the weak connection between the distribution and transmission system will reduce the allowable penetration level of DG;

- the system does not have any small signal instability problem.

4.3.2   Strategies to Increase the Penetration Level of DG and the Corresponding Impacts on the Small Signal Stability of the SNI

Methods to Counteract the Steady State Voltage Rise

It is well recognized that the system steady state voltage rise plays an important role on limiting the penetration level of DG. Thus many methods are proposed to cope with this voltage rise effect [67][68][66]:

- if available, tuning the OLTC at the CCP of the transmission and distribution system;
- adopting shunt compensating devices to adjust the reactive power injection;
- when necessary, curtailing the power generation of DG;
- implementing load control;
- selecting proper connection point for DG;
- changing line impedance.

Curtailment of DG power generation does not meet the aim of this work; load control may not be feasible when suitable loads, such as thermal storage heaters, are not available; considerations on network topology and parameters, such as the selection of DG connecting point and changing line impedance, are apparent to be predicted with positive contributions to the small signal stability. Thus, the focus will be put on the first two methods, i.e., using OLTC and shunt compensators for voltage control.

Further, compared to shunt compensators, the OLTC is foreseen to play an ancillary role in this work. The reasons are: on the one side, DG has a stochastic output, thus when its penetration level is high, it will cause relatively large voltage fluctuations; on the other side, the response of the OLTC is relatively slow, which can be tens even up to hundreds of seconds. These two sides lead to a potential risk that before the proper operations of the OLTC, the system has already subjected to an unallowable overvoltage lasted for an unallowable period. Thus the functions of the OLTC in this work are simplified as: when the load level is low, the OLTC makes the voltage of the CCP equal to 1.0; while when the load level is high, the OLTC makes the voltage of the CCP equal to 1.05.

As for shunt compensating devices, STATCOM stands out from all the candidates for its better operation characteristics, such as improved V-I relation, faster response time and so on [69][70]. Hence it is adopted here to control the steady state voltage. The relevant parameters are reported in appendix D.

Design of the Control Strategy of STATCOM

As discussed in [71] and [7], the so-called unity power factor (UPF) strategy does not help much to increase the penetration level of WGS. Under some specific conditions it may even adversely affect system operation characteristics. Thus here the STATCOM is used to control nodal voltage directly rather than aim to correct the power factor and hence affect the nodal voltage indirectly. However, calculations reveal that it is impracticable if the set point of the STATCOM is fixed, say, $V_{tref} = 1.0$. The reason is that the STATCOM does not have enough capacity to maintain the nodal voltage fixed under all scenarios. One apparent solution is to adopt a large capacity STATCOM. However, this may not be economically justifiable. Another solution, which is used here and will be discussed later

in detail, is to employ an adaptive set point adjustment scheme (ASPAS), to adjust the reference voltage according to the operation state of the system.

In this work, it is observed that the fluctuation of the nodal voltage is mainly determined by the power injection from WGS as well as the load level. Further, as for the power generation from the WGS, since the induction generator is employed, the injected reactive power is highly dependent on the injected active power, thus the injected active power can be used as an indicator for the generation level of the WGS. On the other hand, as for the load level, it can be detected by summing up the power injected by WGS and that from the CCP. More simulations further reveal that, if the load level keeps unchanged while the output of WGS changes, though the sum of the reactive power from the WGS and the CCP has a relatively large fluctuation, that of the active power keeps relatively stable. Thus it can be used as an indicator for the load level. Therefore, it is proposed that the set point of the STATCOM can be determined according to both the active power fed by the WGS and the sum of the active power from the WGS and the CCP.

The implementation of the ASPAS works as follows: assuming a rough relation is available, which maps the active power of WGS and the sum of the corresponding active power to an expected STATCOM set point, then if the operation state of the system changes, a rough value of the reference voltage can be determined by referring to the relation, which later will be called as a map. Based on it, if the operation state of the STATCOM does not meet the prescribed criterion, the set point will further be stepwise tuned.

Map of the Active Power by the WGS and the Sum of the Active Power from the WGS and the CCP to the set point of the STATCOM

The map consists of 2 components:

- A basic frame of the map —- The frame is actually a set of the precalculated solutions of the STATCOM set point for some typical scenarios.

- Rules to get the solution of the set point for real cases —- In this work, when the real operation state of the system is available, linear interpolations are used to get the solution from the above mentioned basic frame.

To form the basic frame of the map, the following factors/assumptions are considered:

- In the precalculated scenarios, two parameters vary from case to case. They are: 1. the load level, which has options as being a minimum load demand or a maximum load demand; 2. the wind speed, which can have a value from the set [0 0.4 0.5 0.6 0.7 0.8 0.9 1.0]. Thus there are totally 16 precalculated scenarios.

- The value of the STATCOM set point is assumed to have a resolution as 0.01 p.u., i.e., the value of the set point can be, for example, 0.95 or 0.96, but can not be 0.955.

- Under steady state, the STATCOM is allowed at most to provide/absorb a quantity of reactive power equal to 70% of its capacity. This guarantees that generally the STATCOM will have at least 30% of the reactive power capacity as a reservation, which may be very helpful for dealing with some emergent situations.

- The STATCOM set point of the precalculated scenarios is determined by the policy of maximizing the reservative capacity of the STATCOM.

After the mapping, the obtained solution of the set point will be further stepwise tuned if necessary. The assumptions during the tuning are:

- The discrete tuning step is 0.01 p.u., however, the set point can not be lower than 0.9 p.u. or higher than 1.1 p.u..

- The STATCOM must have at least 30% reservative capacity under the steady state.

Results and Analyses

In order to make the study concise, by referring to previous results, it is assumed that all the WGS and the STATCOM are connected to node 890. Simulations show that for the scenarios of group 1 and 2 given in table 4.1, totally 9 WGS can be connected; while for the scenarios of group 3 and 4, the corresponding penetration level is 8 WGS.

The above mentioned map for determining the set point of the STATCOM is given in fig. 4.10(*a*) and (*b*) for group 1,2 and 3,4 respectively.

More details about fig. 4.10 are given as:
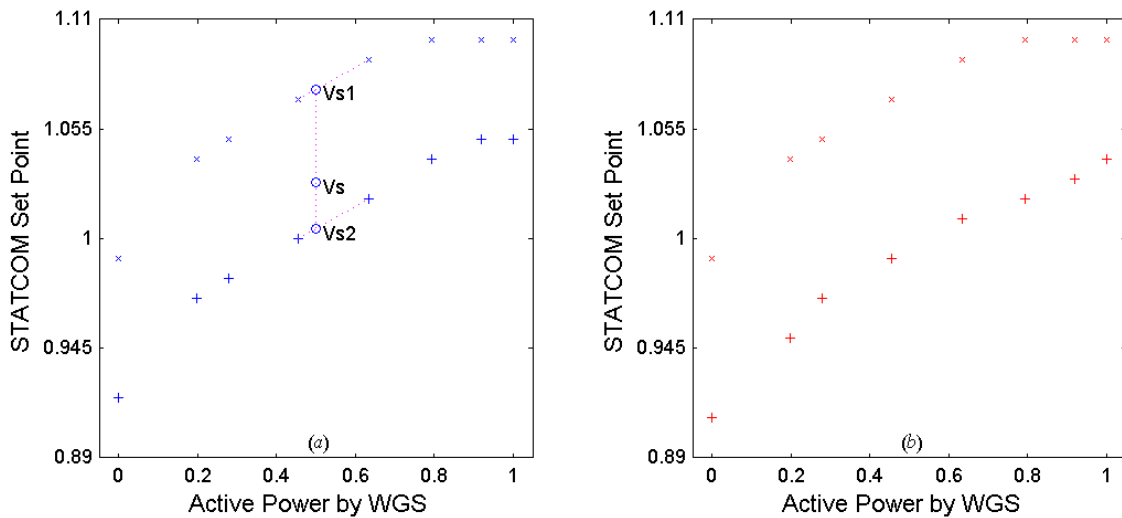
Figure 4.10: Strategy for STATCOM set point

- The basic frame are a set of the solutions of the set point marked by markers '+' and 'x', where, markers '+' designate the STATCOM set point when the load level is low while markers 'x' specify the set point when the load level is high.

- The active power shown in the figure and later discussion is scaled by the total capacity of the installed WGS, which in this part for scenario group 1 and 2 is 18 MVA while for scenario group 3 and 4 is 16 MVA.

- The implementation of the rules to get the solution of the set point for a real case is explained via an example given in fig. 4.10(a). Assuming an actual system operation state is known as: 1. the active power from the WGS is 0.5; 2. the sum of the active power from the WGS and the CCP is 0.75. As previously discussed, the sum of the active power from the WGS and the CCP is the indicator of the load level. Thus condition 2 can be rewritten as the load level is about 0.75. According to the first condition, points Vs1 and Vs2 are obtained by linear interpolation. For Vs1, it corresponds to the operation state as the active power from the WGS is 0.5, while the load level is 1.0 (a maximum load demand). For Vs2, it corresponds to the operation state as the active power from the WGS is 0.5, while the load level is 0.2 (a minimum load demand). By linear interpolation according to the second condition, the expected STATCOM set point Vs is obtained from Vs1 and Vs2, which has a value about 1.03.

Other relevant simulation results are:

- for scenario group 1,

  the conditions for the worst scenario: the WGS produces full power generation; the voltage of the STATCOM set point equals 1.05;

  the damping ratio of the CRE: 0.0757;

  the corresponding CRE: -0.312 $\pm$ j4.116.

- for scenario group 2,

  the conditions for the worst scenario: the WGS produces full power generation; the voltage of the STATCOM set point equals 1.1;

  the damping ratio of the CRE: 0.0651;

  the corresponding CRE: -0.269 $\pm$ j4.129.

- for scenario group 3,

  the conditions for the worst scenario: the WGS produces full power generation; the voltage of the STATCOM set point equals 1.04;

  the damping ratio of the CRE: 0.0780;

  the corresponding CRE: -0.321 $\pm$ j4.108.

- for scenario group 4,

  the conditions for the worst scenario: the WGS produces full power generation; the voltage of the STATCOM set point equals 1.1;

  the damping ratio of the CRE: 0.0650;

  the corresponding CRE: -0.269 $\pm$ j4.126.

The results demonstrate that the installation of the STATCOM increases the penetration level of WGS. Meanwhile, as for the aspect of the small signal stability, it has been improved when using the CRE and their damping ratio as an evaluation criterion.

4.3.3   Relevant Results for the SNII

When investigating the impacts of WGS on the small signal stability of the SNII, 3 factors are expected to have a relatively large influence on the results, i.e., load level, WGS penetration level and WGS generation level. The considerations for them are similar as those

in the previous part. The main difference is about the load level, for which, a low load level here corresponds to the load values in appendix C, while a high load level means the magnitude of the load is 5 times bigger than that of the low load level.

Similar as in the previous part, according to the criterion of the steady state nodal voltage, the maximum number of WGS allowed to connect to the SNII is determined as 3. It is worth noting that in the relevant analyses, both node 1 and 2 of the SNII are modeled as slack buses, and the difference of the voltage angles between them is determined by a preliminary power flow calculation under the assumptions as:

- without DG
- with a low load level
- the active power injection from node 1 is 1.3 MW
- the magnitude of the voltages at node 1 and 2 is 1.05 p.u..

As for the small signal stability, the worst scenarios and their corresponding conditions are given in the following:

- When the load level is low,

  the conditions for the worst scenario:

13	13	13	1	1	1

  the damping ratio of the CRE: 0.0586

  the corresponding CRE: -0.247 $\pm$ j4.209

- When the load level is high,

  the conditions for the worst scenario:

13	13	13	1	1	1

  the damping ratio of the CRE: 0.0595

  the corresponding CRE: -0.251 $\pm$ j4.208

When a STATCOM is installed, which together with the WGS is assumed to be connected to node 13, the following results are obtained:

- The maximum number of WGS allowed to connect to the system is 4

- When the load level is low,

  the conditions for the worst scenario: the WGS produces full power generation; the

  voltage of the STATCOM set point equals 1.1;

  the damping ratio of the CRE: 0.0624

  the corresponding CRE: -0.260 $\pm$ j4.157

- When the load level is high,

  the conditions for the worst scenario: the WGS produces full power generation; the

  voltage of the STATCOM set point equals 1.08;

  the damping ratio of the CRE: 0.0672

  the corresponding CRE: -0.283 $\pm$ j4.200

From the results it can be seen that generally the integration of WGS will not result in small signal instability problems. The installation of STATCOM helps to increase the penetration level of WGS as well as improve the small signal stability of the whole system. These conform to the conclusions obtained in the previous part.

4.3.4   Conclusions and Comments

This chapter focuses on studying the impacts of DG on the small signal stability of distribution systems. The simulations lead to the following conclusions:

- A high penetration level of DG will not lead to small signal instability problems. Compared to the small signal stability, the steady state voltage rise of the system is a more important factor to determine the penetration level of DG.

- The worst case of the small signal stability happens when the following conditions are met: 1. all the DG are connected to a node which has a weak connection to the network; 2. the power generation level of the DG is high; 3. the load level is low.

- Suitable reactive compensations are helpful for the integration of DG. In this work, the application of STATCOM increases the penetration level of DG while at the same time improves the small signal stability of the whole system.

So far, some instructive conclusions are obtained. However, some limitations about the results exist as well. They are:

- The results obtained in this chapter are based on the assumption that the system is three phase symmetric and balanced. These are common assumptions when adopting the modal analysis to investigate the small signal stability. In case the unsymmetric structure or the unbalanced operation is too heavy to be omitted, some other more sophisticated theories have to be adopted.

- In this work, the DG are confined to the constant speed wind generation systems. To get more general conclusions, an apparent solution is developing a universal model of DG to execute the corresponding analyses. However, the development of such a model will be a demanding task, not only because of the various characteristics of different types of DG, but also the lack of practical data. The deficiency of the necessary data will also challenge the verification of the universal model (if available). All in all, to develop an universal model is very helpful if not indispensable, but it is hard to be achieved because of the limited resources at the present stage and can constitute a core part of the future work.

- It is well known that the normal way of wind generation is to collect several wind turbines together to form a wind farm to generate and feed electricity into the network. Thus the investigations in section 4.3.1 about each WGS connected to a different node seems not to agree with the practical situation. Besides, assuming the wind blown on each wind turbine has totally independent speed also does not agree with the real situation. However, since the object of this work is to evaluate the impacts of DG rather than only WGS on system operations in a more general sense, to allow the WGS to be connected to the network arbitrarily and at the same time have totally independent power generation levels (equivalent to totally independent wind speeds) may give a more suitable approximation to the potential operation of DG in the future thus leads to some more general conclusions.

- In section 4.3.2, the operation of the OLTC has been simplified. Efforts can be made in the future to coordinate the OLTC and the STATCOM more effectively to increase the penetration level of DG as well as improve the system operations.

Chapter 5

Impacts of DG on the Voltage Stability of Distribution Systems

Voltage stability refers to the ability of a power system to maintain steady voltages at all buses in the system after being subjected to a disturbance from a given initial operating condition. It is reasonable to expect that the installation of DG will enhance the voltage stability of a distribution system. In this chapter, this conjecture will be verified with the method of continuation power flow to investigate the voltage stability margin improvement after the integration of DG. Further, the effectiveness of some possible operation modes of DG on the improvement of the voltage stability is discussed.

In this chapter, section 5.1 presents a detailed description of the implementation of the continuation method. Section 5.2 gives information about the assumptions and models for the analyses in this chapter. Simulations, results and comments are available in section 5.3.

The work of this chapter shows that the integration of DG is helpful to improve the voltage stability of distribution systems. Further, DG operation mode has a great influence on the improvement of the voltage stability. The greatest improvement is obtained when the DG is operated under the constant nodal voltage mode.

5.1 Implementation of the Continuation Method

Continuation methods are important tools for implementation of branch tracing or path following. A most frequently and successfully used continuation method may be the one based on a so-called 'predictor - corrector' procedure. [72] well documents its application on general nonlinear systems. While [73] [74] [75] thoroughly describe the way of its implementation in power system analyses. In the following, its principles are reviewed in detail by taking power systems as an example.

A quasi steady power system can be modeled as

$$0 = f(\mathbf{x}, \lambda) \tag{5.1}$$

where, $\mathbf{x}$ is a n-dimensional vector, and depending on the modeling level, $\mathbf{x}$ can only include nodal voltages and corresponding angles, or further consist of some state variables; while λ is normally a scalar variable to be used to control a continuative variation of certain parameters.

For example, when investigating the power system loadability on a peculiar direction, the system load can be modeled as:

$$
\begin{aligned}
\mathbf{P}_L &= \mathbf{P}_{L_0} + \lambda \mathbf{P}_d \\
\mathbf{Q}_L &= \mathbf{Q}_{L_0} + \lambda \mathbf{Q}_d
\end{aligned}
\tag{5.2}
$$

where $\mathbf{P}_{L_0}$ and $\mathbf{Q}_{L_0}$ are the original load of the system; while $\mathbf{P}_d$ and $\mathbf{Q}_d$ designate a particular direction of load variation.

In order to find a solution of eqn. (5.1), firstly a guess of the solution must be made (this actually is done by the predictor), then from the guess (the initial value) the real solution has to be found (this is fulfilled by the corrector). The following parts give the details of this procedure.

Predictor

Predictors normally can be divided into two classes:

- ODE-based method —- This method exploits the current solution and the concerned derivatives to form the initial guess of the next solution. When only the first order derivative is used, it forms the so-called tangent predictor.

- Polynomial extrapolation based method —- This method uses the current as well as the previous solutions to predict the next solution. When a zero order polynomial is adopted, this method equals to take the present solution directly as the initial guess of the next solution. When a first order polynomial (a line) is adopted, it leads to the so-called secant predictor.

Tangent Predictor

Differentiating eqn. (5.1) leads to

$$0 = f_{\mathbf{x}} d\mathbf{x} + f_{\lambda} d\lambda \tag{5.3}$$

where $f_{\mathbf{x}}$ and f_{λ} are the corresponding Jacobian matrices.

When $f_{\mathbf{x}}$ is nonsingular, eqn. (5.3) leads to

$$\frac{d\mathbf{x}}{d\lambda} = -(f_{\mathbf{x}})^{-1} f_{\lambda} \tag{5.4}$$

Note that eqn. (5.4) gives a increment direction of $\mathbf{x}$ when λ increases. Assuming the present solution as $(\mathbf{x}_0, \lambda_0)$, given a stepsize as $\Delta\lambda$, thus the increment of $\mathbf{x}$ is

$$\Delta\mathbf{x} = -(f_{\mathbf{x}}|_{\mathbf{x}=\mathbf{x}_0, \lambda=\lambda_0})^{-1} f_{\lambda}|_{\mathbf{x}=\mathbf{x}_0, \lambda=\lambda_0} \Delta\lambda \tag{5.5}$$

and therefore the guess of the next solution can be predicted as

$$
\begin{aligned}
\mathbf{x}_1^p &= \mathbf{x}_0 + \Delta\mathbf{x} \\
\lambda_1^p &= \lambda_0 + \Delta\lambda
\end{aligned}
\tag{5.6}
$$

where, the superscript p means a predicted value.

However, this procedure fails when the bifurcation point is reached, where the Jacobian matrix $f_{\mathbf{x}}$ is singular. This problem can be solved by switching λ in the previous equations to an alternative parameter. It can be achieved as follows:

When the aforesaid procedure approaches the bifurcation point, it is noticed that when λ has a small increment, some other parameters may subject to a sharp change. Under this situation, the one which has the largest relative increment, say x_i, can be used to substitute λ to implement the aforesaid procedure in a similar way.

Eqn. (5.3) will be rearranged as

$$0 = f_{\hat{\mathbf{x}}} d\hat{\mathbf{x}} + f_{x_i} dx_i \tag{5.7}$$

where, $\hat{\mathbf{x}} = [x_1 \ ... \ x_{i-1} \ x_{i+1} \ ... \ x_n \ \lambda]^T$.

Thus the incremental direction of $\hat{\mathbf{x}}$ with respect to x_i is

$$\frac{d\hat{\mathbf{x}}}{dx_i} = -(f_{\hat{\mathbf{x}}})^{-1} f_{x_i} \tag{5.8}$$

Assuming the current solution as $(\hat{\mathbf{x}}_0, x_{i0})$, given a stepsize as Δx_i, hence the corresponding increment of $\hat{\mathbf{x}}$ is

$$\Delta \hat{\mathbf{x}} = -(f_{\hat{\mathbf{x}}}|_{\hat{\mathbf{x}}=\hat{\mathbf{x}}_0, x_i=x_{i0}})^{-1} f_{x_i}|_{\hat{\mathbf{x}}=\hat{\mathbf{x}}_0, x_i=x_{i0}} \Delta x_i \tag{5.9}$$

and therefore the next point can be predicted as

$$\begin{aligned} \hat{\mathbf{x}}_1^p &= \hat{\mathbf{x}}_0 + \Delta\hat{\mathbf{x}} \\ x_{i1}^p &= x_{i0} + \Delta x_i \end{aligned} \tag{5.10}$$

When x_i is properly selected, the Jacobian matrix $f_{\hat{\mathbf{x}}}$ is guaranteed to be nonsingular even at the bifurcation point, thus the feasibility of eqn. (5.9).

Secant Predictor

Assuming the present and previous solutions of eqn. (5.1) are known as $(\mathbf{x}_1, \lambda_1)$ and $(\mathbf{x}_0, \lambda_0)$, then the secant predictor adopts the first order polynomial to predict the next point as:

$$\begin{aligned} \mathbf{x}_2^p &= \mathbf{x}_1 + h(\mathbf{x}_1 - \mathbf{x}_0) \\ \lambda_2^p &= \lambda_1 + h(\lambda_1 - \lambda_0) \end{aligned} \tag{5.11}$$

where, h is a proper stepsize.

Corrector

A corrector is actually an algorithm to solve the real solution $(\mathbf{x}, \lambda)$ of eqn. (5.1) with the available initial guess of $(\mathbf{x}^p, \lambda^p)$, which is from the predictor. Newton method is popularly utilized in various correctors for its effectiveness of solving nonlinear equations.

Observation of eqn. (5.1) shows that it includes n equations but $n + 1$ variables. This means another extra equation is necessary for the solution. The procedure of forming another required equation is called parameterization. The normally used parameterization methods include: 1. local parameterization; 2. perpendicular intersection parameterization; 3. arclength parameterization. In the following they are explained in detail.

Local Parameterization

In local parameterization, either one element of the $n-$dimensional vector $\mathbf{x}$ or the scalar λ is forced to be a fixed value. That is, one of the following equations will be added together with eqn. (5.1) for seeking a practical solution.

$$\lambda - \lambda^p = 0 \tag{5.12}$$

$$x_i - x_i^p = 0 \tag{5.13}$$

Normally eqn. (5.12) is adopted at the beginning of the procedure. With the approaching of the bifurcation point, eqn. (5.13) will be used instead.

Perpendicular Intersection Parameterization

It is assumed that in perpendicular intersection parameterization, for the current solution $(\mathbf{x}_0, \lambda_0)$, the prediction of the next solution $(\mathbf{x}_1^p, \lambda_1^p)$, and the real value of the next solution $(\mathbf{x}_1, \lambda_1)$, the hyperplane determined by $(\mathbf{x}_0, \lambda_0)$ and $(\mathbf{x}_1^p, \lambda_1^p)$ is perpendicular to the one determined by $(\mathbf{x}_1^p, \lambda_1^p)$ and $(\mathbf{x}_1, \lambda_1)$. That is, the following condition is a complement of eqn. (5.1).

$$[\mathbf{x}_1^p - \mathbf{x}_0]^T * [\mathbf{x}_1 - \mathbf{x}_1^p] + (\lambda_1^p - \lambda_0) * (\lambda_1 - \lambda_1^p) = 0 \tag{5.14}$$

Arclength Parameterization

The arclength parameterization method introduces the arclength s on the solution curve as a new parameter. From the current solution $(\mathbf{x}_0, \lambda_0)$ to the next solution $(\mathbf{x}_1, \lambda_1)$, the corresponding increment of the arclength, i.e., Δs, is under control. This leads to the following additional equation for eqn. (5.1).

$$\sum_{i=1}^{n} (x_{i1} - x_{i0})^2 + (\lambda_1 - \lambda_0)^2 - (\Delta s)^2 = 0 \tag{5.15}$$

Step Length Control

One apparent step length control strategy is to take a constant step length, say, with $\Delta \lambda = 0.1$ during the procedure. If the step length is small enough, it may work successfully for a wide range of problems. However this will often lead to inefficient computation, since too many steps are spent on the 'flat' part of the solution curve. On the contrary, if a larger step length is adopted, though the time for branch tracking on the flat part may be reduced, when the curvature increases, it can cause the predicted value (from the predictor) deviating far from the true solution, thus the time for the corrector computation increases. In some extreme case, the corrector may even be subjected to divergence. All these imply that an adaptive step length control strategy has to be used.

In [72], it is pointed out that "the total amount of work of a continuation procedure depends on the average step length in a somewhat convex manner: The continuation is expensive both for very short steps (too many steps) and for very large steps (slow or no convergence of the corrector). Its costs are moderate for a certain medium step length, which is related to an optimal number N_{opt} of iterations of a corrector" (quoted from [72]). Thus the relation of the predetermined N_{opt} and the actual iteration number N_j of the present corrector computation can be adopted to adjust the step length for the next computation adaptively. When $N_{opt} > N_j$, the step length is considered to be increased; while when $N_{opt} < N_j$, it will be reduced .

Another option of step length control strategy may take the curvature of the solution curve into account as well. This can be done by assuming λ is the controlled continuative parameter, thus the scaled directions of $\mathbf{x}$ with respect to λ at the previous solution of

$(\mathbf{x}_0, \lambda_0)$ and the current solution of $(\mathbf{x}_1, \lambda_1)$ can be used to determine the step length as

$$h = \frac{h_c}{||J_1 - J_0||} \tag{5.16}$$

where J is the scaled direction, h_c a constant mainly depending on experience, h the step length, which in practice may be bounded, say, as

$$h = \begin{cases} 0.1 & \text{if } h < 0.1 \\ h & \text{if } 0.1 \leq h \leq 1 \\ 1 & \text{if } h > 1 \end{cases} \tag{5.17}$$

Eqn. (5.16) reveals that at the flat part of the solution curve, since the directions will not change so much, their difference thus will be relatively small, therefore a large step length is obtained. However, when the curve turns sharply, the distance between two scaled directions increases quickly as well, thus a small step length is accordingly adopted.

5.2   Models of Power System Components

In this chapter, the steady state models are used:

- **The transmission system** is modeled as an infinite bus.

- **The electrical network** is mathematically modeled as a nodal admittance matrix.

- **The load** is modeled as a constant PQ component.

- **The DG** is modeled as a PQ generator. However, when enough capacities of the shunt compensator are assumed in operation, they together will be modeled as a PV generator.

The DG is modeled as a PQ generator because normally it is not controlled by system operators. This model may be suitable for those types of DG which have relatively stable performance, such as fuel cell generations and combined heat and power plants. But for other DG, such as WGS and photovoltaic generation systems, it is not true. However, with the development of various feasible energy storage systems, the output of the aforesaid DG may be expected to be well stabilized in the future, thus makes the PQ model to be acceptable.

5.3   Simulations and Results

Impacts of DG on the Voltage Stability of the SNI

Based on the discussion of the previous chapter, the following assumptions are adopted to make the analyses concise as well as meaningful.

- The voltage at the node 800 is fixed as 1.05 p.u..

- The DG is connected to node 890, which has an output of the active power as 12MW. However, the corresponding reactive power is determined according to three options of the power factor: unitary power factor, capacitive power factor 0.95 and inductive power factor 0.95.

- The parameters of the load given in appendix B are adopted here as the load variation direction. Hence in the following analysis, the load is changed as:

$$
\begin{aligned}
P_L &= \lambda P_{L_0} \\
Q_L &= \lambda Q_{L_0}
\end{aligned}
\tag{5.18}
$$

  where λ is a positive real number. P_{L_0} and Q_{L_0} are the initial conditions of the load given in the precious chapter.

After the continuation power flow calculation, the relation between the nodal voltage of bus 890 and the total active power of the load is presented in fig. 5.1, which reveals that generally the integration of DG is helpful for the voltage stability of the distribution system. Further, the largest gain of the voltage stability margin is obtained when the connected DG is operated under the capacitive power factor mode.

If enough shunt compensators are installed for nodal reactive power injection control, then they may offer another optional operation mode – keep the concerned nodal voltage constant. Compared to the capacitive power factor mode, this mode can make the voltage stability properties even better. Fig. 5.2 shows the results using the relation of the nodal voltage of bus 888 and the total active power of the load as an example, where the nodal voltage 890 is assumed to be as 1.05 p.u.. Besides, the corresponding curve of the aforementioned capacitive power factor mode is also drawn in it for convenience of comparison.
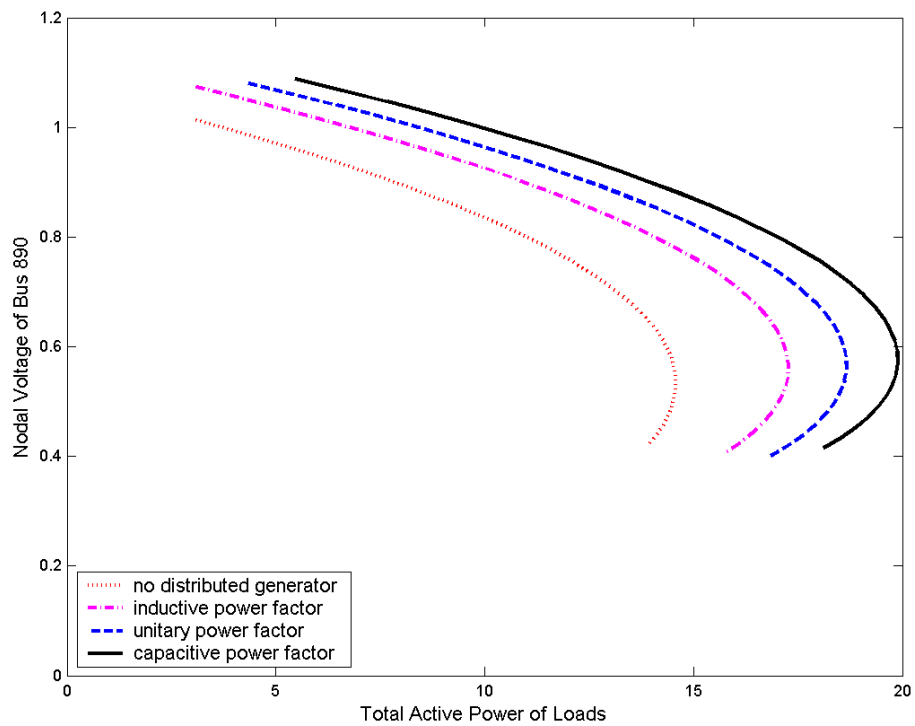
**Figure 5.1:** Loadability of the SNI for DG under different operation modes
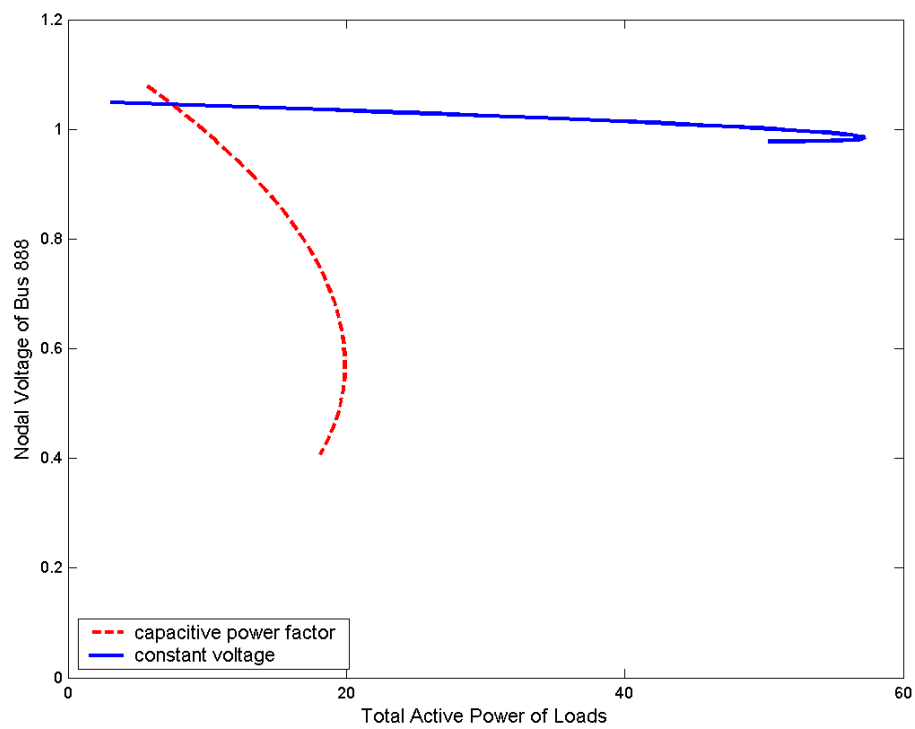
Figure 5.2: Comparison of the loadability of the SNI for DG under the operation modes
of constant voltage and capacitive power factor

Impacts of DG on the Voltage Stability of the SNII

Similar as in the previous part, some assumptions are adopted here to simplify the analyses:

- The voltage at the node 1 and 2 are fixed as 1.05 p.u., and the difference of their arguments is also fixed. Further, when enough shunt compensation is available, the concerned nodal voltage is assumed to be 1.05 p.u..

- The DG as well as the shunt compensator (if available) is connected to node 13. The active power output of the DG is 6MW. There are 4 options of the operation mode: unitary power factor, capacitive power factor 0.95, inductive power factor 0.95 and constant voltage.

- The parameters of the load given in appendix C are the load variation direction.

Fig. 5.3 gives the results of the continuation power flow analyses for the scenarios of without DG and DG as a PQ generator. Since the SNII is fed of electricity by the transmission system simultaneously at two nodes, its voltage stability is much better compared to that of the SNI. In fig. 5.3, only part of the whole P-V curve for node 13 is given. To compute a complete P-V curve is not necessary, since the bifurcation point of the SNII will appear when the load is so heavy as to override the thermal limit of the cable. Thus to determine such a bifurcation point is physically meaningless. Without information about the location of the bifurcation point, an obvious observation about the voltage stability improvement is not available. However, fig. 5.3 shows that the nodal voltage of bus 13 is increased after the integration of the DG, hence it is reasonable to expect that the voltage stability of the whole system has been improved.

As for the scenarios of the DG modeled as a PV generator, the results are given in fig. 5.4. It indicates that compared to the mode of capacitive power factor, when the DG is operated under the constant voltage mode, the nodal voltage drop will be smaller as the increment of the load level. Thus it is reasonable to predict that the constant voltage mode will be more helpful for the voltage stability of the system.
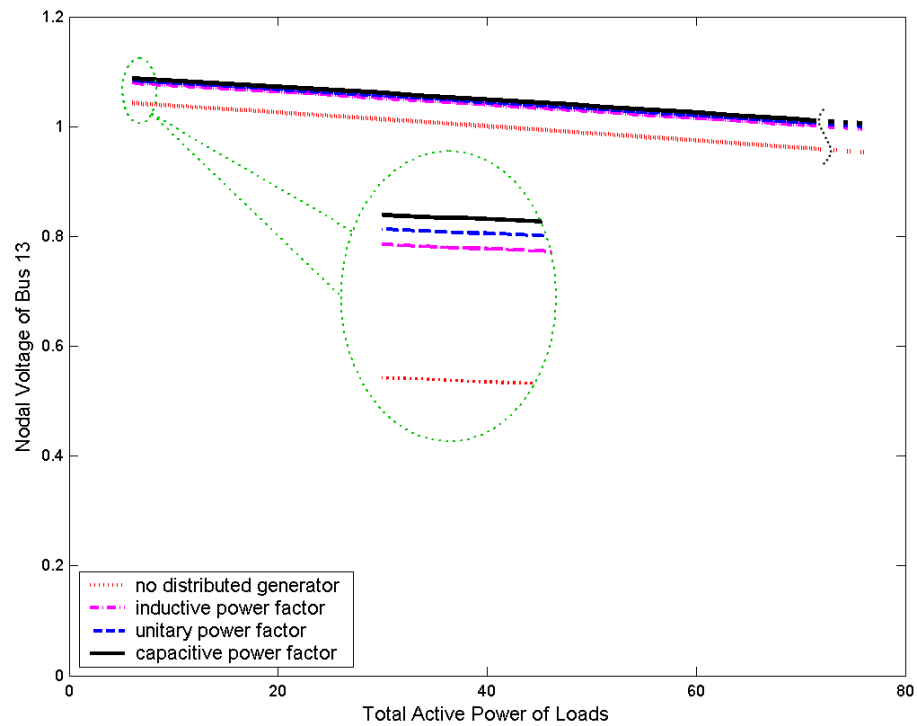
Figure 5.3: Loadability of the SNII for DG under different operation modes
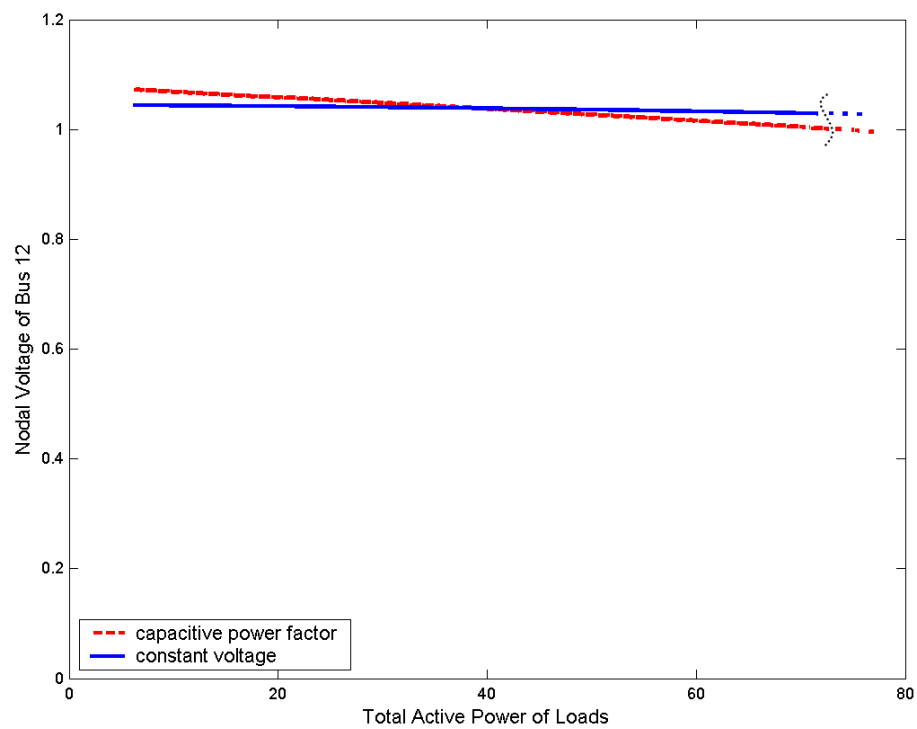
Figure 5.4: Comparison of the loadability of the SNII for DG under the operation modes

of constant voltage and capacitive power factor

Comments

So far, a positive expectation of DG to improve the voltage stability is given. However, this work may be improved when the following aspects are taken into account:

- As in the previous chapter, the results obtained in this chapter are also based on a three phase symmetric system under balanced operation. In case of investigations under unsymmetric structure or unbalanced operation, methods proposed in [76] are applicable.

- Compared to traditional electricity generation, the operation of DG contains more stochastic characteristics. Thus to investigate their impacts on the voltage stability from a more stochastic standpoint may be more suitable and helpful. However, research in this aspect is still open since the lack of practical experience and data.

Chapter 6

Conclusions and Future Works

6.1   Conclusions

Concerning **the studies of the eigenvalues of the state space model of distribution networks**, the following conclusions are drawn:

- There is a close relation between the eigenvalues of the network under *abc* and *dq*0 reference frame. Assuming a symmetric network has $3N$ state variables, thus it has $3N$ eigenvalues. Among them, N pairs of the complex-conjugate/double-real eigenvalues under *abc* frame, relate only to the network *dq* components under *dq*0 frame. These eigenvalues under *dq*0 frame can be gotten by shifting the counterparts under *abc* frame with frequency of $\pm\omega_0$. The remaining N eigenvalues will keep unchanged under both of the two frames.

- The parameters of the lines/cables of the electrical network are the predominant factors to determine the eigenvalues of the network. Although the network topology has an influence on the eigenvalues, the parameters of the lines/cables are of much greater influence.

- The distribution of the eigenvalues of the network is bounded by the relevant values of its lines/cables. Assuming a distribution network consists of M different types of lines, then the maximum and minimum values of the real parts of their CE span a range, which covers the total interval spanned by the real parts of the CE of the network.

- In a real distribution network in Europe, the eigenvalues will have the real parts within the range from -69.3 to -33055. This is based on a thorough investigation of the data of the lines/cables given in Neplan [46].

- The impacts of the apparently successive stochastic disturbances to the network can be studied independently and the nodal admittance matrix is acceptable as the model of a distribution network. The investigation on the eigenvalues of a distribution network reveals that the electrical dynamics die off very fast. Hence a steady state assumption for modeling the distribution network is acceptable. The apparently successive stochastic disturbances have nearly independent influences on the network.

Concerning **the impacts of DG on the small signal stability of distribution systems**, the following conclusions are drawn:

- A high penetration level of DG will not lead to small signal instability problems. Compared to the small signal stability, the steady state voltage rise of the system is a more important factor to determine the penetration level of DG.

- The worst case of the small signal stability happens when the following conditions are met: 1. all the DG are connected to a node which has a weak connection to the network; 2. the power generation level of the DG is high; 3. the load level is low.

- Suitable reactive compensations are helpful for the integration of DG. In this work, the application of STATCOM increases the penetration level of DG while at the same time improves the small signal stability of the whole system.

Concerning **the impacts of DG on the voltage stability of distribution systems**, the following conclusions are drawn:

- In general the integration of DG improves the voltage stability of the distribution system.

- The operation mode of DG has a great influence on the improvement of the voltage stability. The largest gain of the voltage stability margin is obtained when the connected DG is operated under the constant nodal voltage mode.

6.2   Future Works

Works carried out to present stage result in some useful conclusions. However, improvements are expectable in various aspects. Following comments give some indications for the future works in general.

- **Development of a universal model of DG** - A universal model of DG is very helpful if not indispensable for concerned analyses. Though presently hard to achieve, with the accumulation of practical data and experience, it may be feasible in the future.

- **More proper considerations of the stochastic characteristics of DG** - Compared to conventional generation, DG is more stochastic in its operation. Efforts to include this aspect more properly in concerned analyses are meaningful.

- **Researches under three phase unsymmetric/unbalanced conditions** - Distribution systems are apt to be subjected to unsymmetric/unbalanced conditions when compared to transmission systems. Thus researches carried on under these conditions will be more helpful for utilities. However, this is by no means an easy work. New and appropriate methods for this aim may need to be developed.

Appendix

A.   Explanation of Equation (3.13)

Observation

For networks with a radial structure, if the shunt admittance of their lines/cables is negligible, then through a systematic routine their state matrix can be formed in a generalized form as:

$$\dot{\mathbf{I}}_{2(n-1)\times 1} = \mathbf{A}_{2(n-1)\times 2(n-1)}\mathbf{I}_{2(n-1)\times 1} + \mathbf{B}_{2(n-1)\times 2}\mathbf{v}_{2\times 1} + \mathbf{C}_{2(n-1)\times 2(n-1)}\mathbf{V}_{2(n-1)\times 1} \quad (1)$$

where

n is the total number of the nodes of the network;

$\mathbf{I}$ is the set of the state variables consisting of the dq components of the deliberately selected branch currents;

both $\mathbf{v}$ and $\mathbf{V}$ are sets consisting of the dq components of the specially selected nodal voltages.

Example

The network given in fig. 1 is adopted as an example to explain the observation, in which, node 1 is a SN, node 4 and 5 are TN, and node 2, 3, 6, 7 and 8 are EN.

For the structure enclosed by the dotted curve in fig. 1, the following equations are valid:

$$\begin{cases} \frac{L_6}{\omega_0}\frac{di_{6d}}{dt} - L_6 i_{6q} + R_6 i_{6d} &= v_{5d} - v_{6d} \\ \frac{L_6}{\omega_0}\frac{di_{6q}}{dt} + L_6 i_{6d} + R_6 i_{6q} &= v_{5q} - v_{6q} \end{cases} \quad (2)$$

$$\begin{cases} \frac{L_7}{\omega_0}\frac{di_{7d}}{dt} - L_7 i_{7q} + R_7 i_{7d} &= v_{5d} - v_{7d} \\ \frac{L_7}{\omega_0}\frac{di_{7q}}{dt} + L_7 i_{7d} + R_7 i_{7q} &= v_{5q} - v_{7q} \end{cases} \quad (3)$$

$$\begin{cases} \frac{L_8}{\omega_0}\frac{di_{8d}}{dt} - L_8 i_{8q} + R_8 i_{8d} &= v_{5d} - v_{8d} \\ \frac{L_8}{\omega_0}\frac{di_{8q}}{dt} + L_8 i_{8d} + R_8 i_{8q} &= v_{5q} - v_{8q} \end{cases} \quad (4)$$

$$\begin{cases} \frac{L_5}{\omega_0}\frac{di_{5d}}{dt} - L_5 i_{5q} + R_5 i_{5d} &= v_{4d} - v_{5d} \\ \frac{L_5}{\omega_0}\frac{di_{5q}}{dt} + L_5 i_{5d} + R_5 i_{5q} &= v_{4q} - v_{5q} \end{cases} \quad (5)$$
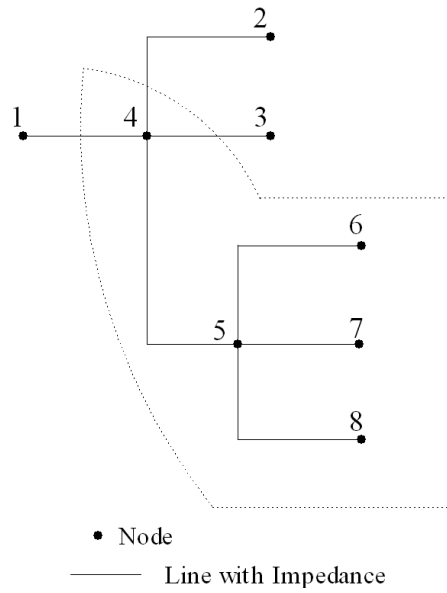
Figure 1: Example for explanation of the general form of state matrix of radial impedance networks

with algebraic equations

$$
\begin{aligned}
i_{5d} &= i_{6d} + i_{7d} + i_{8d} \\
i_{5q} &= i_{6q} + i_{7q} + i_{8q}
\end{aligned}
\tag{6}
$$

where

i_m ($m = 5,6,7,8$) are branch currents flowing from the SN to the TN, or from the TN to the EN;

R_m and L_m are the corresponding branch impedance.

For example, i_5 is the current on the branch with a direction from node 4 to 5, while R_5 and L_5 the corresponding impedance.

It can be noticed that equations (2),(3) and (4) have the following general form

$$
\dot{\mathbf{I}}_i = \mathbf{A}_i \mathbf{I}_i + \mathbf{B}_i \mathbf{V}_{start} + \mathbf{C}_i \mathbf{V}_{end}
\tag{7}
$$

where

$$
\mathbf{A}_i = \begin{bmatrix} -\frac{R_i \omega_0}{L_i} & \omega_0 \\ -\omega_0 & -\frac{R_i \omega_0}{L_i} \end{bmatrix}, \ \mathbf{B}_i = \begin{bmatrix} \frac{\omega_0}{L_i} & \\ & \frac{\omega_0}{L_i} \end{bmatrix}, \ \mathbf{C}_i = -\begin{bmatrix} \frac{\omega_0}{L_i} & \\ & \frac{\omega_0}{L_i} \end{bmatrix}
$$

$i = 6, 7, 8$

and the contents of $\mathbf{I}_i, \mathbf{V}_{start}, \mathbf{V}_{end}$ can be clarified via taking eqn. (2) as an example, in which, $\mathbf{I}_i = [i_{6d}\ i_{6q}]^T$, $\mathbf{V}_{start} = [v_{5d}\ v_{5q}]^T$ and $\mathbf{V}_{end} = [v_{6d}\ v_{6q}]^T$.

Then equations (2),(3) and (4) can be organized as

$$\dot{\mathbf{I}}_{678} = \mathbf{A}_{678}\mathbf{I}_{678} + \mathbf{B}_{678}\mathbf{V}_5 + \mathbf{C}_{678}\mathbf{V}_{678} \tag{8}$$

where

$$\mathbf{A}_{678} = \begin{bmatrix} \mathbf{A}_6 & & \\ & \mathbf{A}_7 & \\ & & \mathbf{A}_8 \end{bmatrix}, \mathbf{B}_{678} = \begin{bmatrix} \mathbf{B}_6 \\ \mathbf{B}_7 \\ \mathbf{B}_8 \end{bmatrix}, \mathbf{C}_{678} = \begin{bmatrix} \mathbf{C}_6 & & \\ & \mathbf{C}_7 & \\ & & \mathbf{C}_8 \end{bmatrix}$$

$\mathbf{I}_{678} = [i_{6d}\ i_{6q}\ i_{7d}\ i_{7q}\ i_{8d}\ i_{8q}]^T$

$\mathbf{V}_5 = [v_{5d}\ v_{5q}]^T$

$\mathbf{V}_{678} = [v_{6d}\ v_{6q}\ v_{7d}\ v_{7q}\ v_{8d}\ v_{8q}]^T$

From eqn. (5) and (6) the following equation can be deduced

$$\mathbf{V}_5 = \mathbf{D}\mathbf{V}_4 + \mathbf{E}_i\dot{\mathbf{I}}_{678} + \mathbf{F}_i\mathbf{I}_{678} \tag{9}$$

where

$$\mathbf{D} = \begin{bmatrix} 1 & \\ & 1 \end{bmatrix}, \mathbf{E}_i = -\frac{L_i}{\omega_0}\begin{bmatrix} 1 & & 1 & & 1 & \\ & 1 & & 1 & & 1 \end{bmatrix}$$

$$\mathbf{F}_i = -R_i\begin{bmatrix} 1 & & 1 & & 1 & \\ & 1 & & 1 & & 1 \end{bmatrix} + L_i\begin{bmatrix} & 1 & & 1 & & 1 \\ -1 & & -1 & & -1 & \end{bmatrix}$$

$\mathbf{V}_4 = [v_{4d}\ v_{4q}]^T$

with $i = 4$.

Eqn. (8) and (9) result

$$\dot{\mathbf{I}}_{678} = \bar{\mathbf{A}}_{678}\mathbf{I}_{678} + \bar{\mathbf{B}}_{678}\mathbf{V}_4 + \bar{\mathbf{C}}_{678}\mathbf{V}_{678} \tag{10}$$

where

$\bar{\mathbf{A}}_{678} = (\mathbf{1}_{6\times 6} - \mathbf{B}_{678}\mathbf{E}_4)^{-1}(\mathbf{A}_{678} + \mathbf{B}_{678}\mathbf{F}_4),$

$$\mathbf{\bar{B}}_{678} = (\mathbf{1}_{6\times6} - \mathbf{B}_{678}\mathbf{E}_4)^{-1}\mathbf{B}_{678}\mathbf{D},$$

$$\mathbf{\bar{C}}_{678} = (\mathbf{1}_{6\times6} - \mathbf{B}_{678}\mathbf{E}_4)^{-1}\mathbf{C}_{678}$$

with

$\mathbf{1}_{6\times6}$ an unit matrix with a dimension of 6×6, superscript -1 the inversion of the corresponding matrix.

The mathematical model of the whole network shown in fig. 1 consists of eqn. (10) as well as the following equations

$$\begin{cases} \frac{L_2}{\omega_0}\frac{di_{2d}}{dt} - L_2 i_{2q} + R_2 i_{2d} &= v_{4d} - v_{2d} \\ \frac{L_2}{\omega_0}\frac{di_{2q}}{dt} + L_2 i_{2d} + R_2 i_{2q} &= v_{4q} - v_{2q} \end{cases} \tag{11}$$

$$\begin{cases} \frac{L_3}{\omega_0}\frac{di_{3d}}{dt} - L_3 i_{3q} + R_3 i_{3d} &= v_{4d} - v_{3d} \\ \frac{L_3}{\omega_0}\frac{di_{3q}}{dt} + L_3 i_{3d} + R_3 i_{3q} &= v_{4q} - v_{3q} \end{cases} \tag{12}$$

$$\begin{cases} \frac{L_4}{\omega_0}\frac{di_{4d}}{dt} - L_4 i_{4q} + R_4 i_{4d} &= v_{1d} - v_{4d} \\ \frac{L_4}{\omega_0}\frac{di_{4q}}{dt} + L_4 i_{4d} + R_4 i_{4q} &= v_{1q} - v_{4q} \end{cases} \tag{13}$$

and

$$\begin{aligned} i_{4d} &= i_{2d} + i_{3d} + i_{6d} + i_{7d} + i_{8d} \\ i_{4q} &= i_{2q} + i_{3q} + i_{6q} + i_{7q} + i_{8q} \end{aligned} \tag{14}$$

Equations (10),(11) and (12) can be arranged as

$$\mathbf{\dot{I}}_{23678} = \mathbf{A}_{23678}\mathbf{I}_{23678} + \mathbf{B}_{23678}\mathbf{V}_4 + \mathbf{C}_{23678}\mathbf{V}_{23678} \tag{15}$$

where

$$\mathbf{A}_{23678} = \begin{bmatrix} \mathbf{A}_2 & & \\ & \mathbf{A}_3 & \\ & & \mathbf{\bar{A}}_{678} \end{bmatrix}, \mathbf{B}_{23678} = \begin{bmatrix} \mathbf{B}_2 \\ \mathbf{B}_3 \\ \mathbf{\bar{B}}_{678} \end{bmatrix}, \mathbf{C}_{23678} = \begin{bmatrix} \mathbf{C}_2 & & \\ & \mathbf{C}_3 & \\ & & \mathbf{\bar{C}}_{678} \end{bmatrix}$$

$$\mathbf{I}_{23678} = [i_{2d}\ i_{2q}\ i_{3d}\ i_{3q}\ i_{6d}\ i_{6q}\ i_{7d}\ i_{7q}\ i_{8d}\ i_{8q}]^T$$

$$\mathbf{V}_4 = [v_{4d}\ v_{4q}]^T$$

$$\mathbf{V}_{23678} = [v_{2d}\ v_{2q}\ v_{3d}\ v_{3q}\ v_{6d}\ v_{6q}\ v_{7d}\ v_{7q}\ v_{8d}\ v_{8q}]^T$$

Combining eqn. (13) and (14) leads to

$$\mathbf{V}_4 = \mathbf{D}\mathbf{V}_1 + \mathbf{E}_i\dot{\mathbf{I}}_{23678} + \mathbf{F}_i\mathbf{I}_{23678} \tag{16}$$

where

$\mathbf{V}_1 = [v_{1d} \; v_{1q}]^T$

$\mathbf{D}$, $\mathbf{E}_i$, $\mathbf{F}_i$ the same as in eqn. (9) with $i = 1$.

Eqn. (15) and (16) result in

$$\dot{\mathbf{I}}_{23678} = \bar{\mathbf{A}}_{23678}\mathbf{I}_{23678} + \bar{\mathbf{B}}_{23678}\mathbf{V}_1 + \bar{\mathbf{C}}_{23678}\mathbf{V}_{23678} \tag{17}$$

where

$\bar{\mathbf{A}}_{23678} = (\mathbf{1}_{10\times10} - \mathbf{B}_{23678}\mathbf{E}_1)^{-1}(\mathbf{A}_{23678} + \mathbf{B}_{23678}\mathbf{F}_1)$,

$\bar{\mathbf{B}}_{23678} = (\mathbf{1}_{10\times10} - \mathbf{B}_{23678}\mathbf{E}_1)^{-1}\mathbf{B}_{23678}\mathbf{D}$,

$\bar{\mathbf{C}}_{23678} = (\mathbf{1}_{10\times10} - \mathbf{B}_{23678}\mathbf{E}_1)^{-1}\mathbf{C}_{23678}$

with

$\mathbf{1}_{10\times10}$ an unit matrix with a dimension of 10×10.

B.   Data of the SNI

Node	Length(km)	Node	Length(km)	Node	Length(km)
800 - 802	0.7864	802 - 806	0.5273	806 - 808	9.8238
808 - 810	1.7691	808 - 812	11.4301	812 - 814	9.0618
814 - 850	0.0030	816 - 818	0.5212	816 - 824	3.1120
818 - 820	14.6763	820 - 822	4.1880	824 - 826	0.9236
824 - 828	0.2560	828 - 830	6.2302	830 - 854	0.1585
832 - 858	1.4935	834 - 860	0.6157	834 - 842	0.0853
836 - 840	0.2621	836 - 862	0.0853	842 - 844	0.4115
844 - 846	1.1095	846 - 848	0.1615	850 - 816	0.0945
852 - 832	0.0030	854 - 856	7.1111	854 - 852	11.225
858 - 864	0.4938	858 - 834	1.7770	860 - 836	0.8169
862 - 838	1.4813	888 - 890	3.2187	832 - 888	1.6094

Table 1: Line Segment Data

$R = 0.128$ Ohm/km,	$X = 0.122$ Ohm/km,	$B = 116.239$ uS/km
$R_0 = 1$ Ohm/km,	$X_0 = 1$ Ohm/km,	$B_0 = 116.239$ uS/km

Table 2: Parameters of the Line Conductor[†]

Node	Ph-A kVar	Ph-B kVar	Ph-C kVar	Node	Ph-A kVar	Ph-B kVar	Ph-C kVar
844	100	100	100	848	150	150	150

Table 3: Shunt Capacitors

[†] The parameters are got from a cable made in Germany, the type of which is '20kV NEKEBA 3×150'.

Node	P kW	Q kVar	Node	P kW	Q kVar	Node	P kW	Q kVar	Node	P kW	Q kVar
802	275	145	806	275	145	808	80	40	810	80	40
816	25	10	818	170	85	820	845	435	822	675	350
824	245	120	826	200	100	828	55	25	830	485	215
832	75	35	834	890	450	836	610	215	838	140	70
840	470	310	842	45	25	844	4320	3290	846	340	170
848	715	535	854	20	10	856	20	10	858	245	125
860	1740	1060	862	140	70	864	10	5	890	2250	1125

Table 4: Loads

C.   Data of the SNII

Node	Type of the cable	Length(km)	Node	Type of the cable	Length(km)
1 - 3	NAKBA 3×150	0.01	19 - 20	NA2XS(F)2Y 3×1×185	0.9086
3 - 4	NAKBA 3×150	0.2409	20 - 21	NAKBA 3×240	0.2885
4 - 5	NAKBA 3×150	0.226	21 - 22	NAKBA 3×240	0.8286
1 - 6	NAKBA 3×150	0.217	22 - 23	NA2XS(F)2Y 3×1×185	0.3374
6 - 7	NKBA 3×70	0.142	15 - 24	NA2XS(F)2Y 3×1×185	0.7855
7 - 8	NKBA 3×70	0.1334	24 - 25	NA2XS(F)2Y 3×1×185	0.9508
8 - 9	NA2XS(F)2Y 3×1×185	0.0416	25 - 26	NAKBA 3×150	0.4218
9 - 10	NKBA 3×70	0.2549	26 - 27	NAKBA 3×150	0.0982
10 - 11	NKBA 3×70	0.4249	2 - 28	NA2XS(F)2Y 3×1×185	0.4994
11 - 12	NAKBA 3×70	0.3664	28 - 19	NA2XS(F)2Y 3×1×185	0.9216
12 - 13	NAKBA 3×70	0.6168	19 - 29	NA2XS(F)2Y 3×1×185	0.4956
1 - 14	NA2XS(F)2Y 3×1×185	0.2619	29 - 30	NA2XS(F)2Y 3×1×185	0.2
14 - 15	NA2XS(F)2Y 3×1×185	0.4069	30 - 31	NA2XS(F)2Y 3×1×185	0.2
15 - 16	NAKBA 3×150	0.685	20 - 32	NAKBA 3×150	0.0661
16 - 17	NAKBA 3×150	1.6537	20 - 33	NAKBA 3×150	0.2606
17 - 18	NAKBA 3×150	0.71	33 - 34	NAKBA 3×150	0.2034
18 - 19	NAKBA 3×95	0.3076			

Table 1: Line Segment Data

Type of the cable	R (Ohm/km)	X (Ohm/km)	B (uS/km)
NAKBA 3×70	0.446	0.104	103.673
NAKBA 3×95	0.323	0.1	116.239
NAKBA 3×150	0.21	0.094	141.372
NAKBA 3×240	0.13	0.089	169.646
NA2XS(F)2Y 3×1×185	0.164	0.161	127.235
NKBA 3×70	0.271	0.104	103.673

Table 2: Parameters of the Cable

Node	S (kVA)	Node	S (kVA)	Node	S (kVA)	Node	S (kVA)	Node	S (kVA)
3	150	9	30	14	210	25	40	30	30
4	80	10	40	21	30	26	90	31	50
5	120	11	200	22	80	27	50	32	50
7	70	12	20	23	20	28	100	33	100
8	50	13	60	24	60	29	100	34	70

Table 3: Loads[†]

[†] All the loads are assumed to have a power factor of 0.95.

D.   Data for System Components

Variable	Description	Value	Variable	Description	Value
-	rated power	400 MVA	-	rated voltage	25 KV
r_a	armature resistance	0.001 p.u.	x_l	leakage reactance	0.05 p.u.
x_d	d-axis synchronous reactance	1.9 p.u.	M	inertia constant	10 s
x_d'	d-axis transient reactance	0.302 p.u.	D	damping coefficient	10 p.u.

Table 1: Parameters of the Equivalent Synchronous Generator

Variable	Description	Value	Variable	Description	Value
-	rated power	2 MVA	-	rated voltage	25 KV
-	rated wind speed	15 m/s	ρ	air density	1.225 kg/m^3
r_S	stator resistance	0.01 p.u.	x_R	stator reactance	0.1 p.u.
r_R	rotor resistance	0.01 p.u.	x_R	rotor reactance	0.08 p.u.
x_m	magnetizing reactance	3 p.u.	H_{wr}	wind turbine inertia	2.5 s
H_m	rotor inertia	0.5 s	K_s	shaft stiffness	0.3 p.u.
p	number of poles	4	η_{GB}	gear box ratio	1:89
R	blade length	37.5 m	b_c	compensating capacitor	0.5 p.u.

Table 2: Parameters of the Constant Speed Wind Turbine Generation System

Variable	Description	Value	Variable	Description	Value
-	rated power	5 MVar	-	rated AC voltage	2 KV
-	rated DC voltage	4 KV	R_t	AC circuit resistance	0.01 p.u.
X_t	AC circuit reactance	0.1 p.u.	R_{dc}	DC circuit resistance	400 p.u.
C_{dc}	DC circuit capacitance	0.25133 p.u.	K_{acp}	-	10
K_{aci}	-	10	K_{dcp}	-	10
K_{dci}	-	10			

Table 3: Parameters of STATCOM

Bibliography

[1] R.A.Schlueter, G.L.Park, M.Lotfalian, et al, 'Modification of Power System Operation for Significant Wind Generation Penetration', IEEE Transactions on Power Apparatus and Systems, Vol. PAS-102, No.1, pp. 153-161, January 1983.

[2] A. Bhowmik, A. Maitra, S.M. Halpin, J.E. Schatz, 'Determination of allowable penetration levels of distributed generation resources based on harmonic limit considerations', IEEE Transactions on Power Delivery, Vol. 18, pp. 619-624, April 2003.

[3] W. Freitas, J.C.M. Vieira, A. Morelato, W. Xu, 'Influence of excitation system control modes on the allowable penetration level of distributed synchronous generators', IEEE Transactions on Energy Conversion, Vol. 20, pp. 474-480, June 2005.

[4] J.G. Slootweg, 'Wind Power Modelling and Impact on Power System Dynamics', PhD thesis, Technische Universiteit Delft, Netherlands, 2003

[5] R.T. Guttromson, 'Modeling distributed energy resource dynamics on the transmission system', IEEE Transactions on Power Systems, Vol. 17, pp. 1148-1153, November 2002.

[6] M.K. Donnelly, J.E. Dagle, D.J. Trudnowski, G.J. Rogers, 'Impact of the distributed utility on transmission system stability', IEEE Transactions on Power System, Vol. 11, pp. 741-746, May 1996.

[7] W. Freitas, A. Morelato, Wilsun Xu, F. Sato, 'Impacts of AC Generators and DSTAT-COM devices on the dynamic performance of distribution systems' , IEEE Transactions on Power Delivery, Vol. 20, Part 2, pp. 1493-1501, April 2005.

[8] W. Freitas, J.C.M. Vieira, A. Morelato, L.C.P. daSilva, V.F. da Costa, F.A.B. Lemos, 'Comparative Analysis Between Synchronous and Induction Machines for Dis-

tributed Generation Applications', IEEE Transactions on Power Systems, Vol. 21, pp. 301-311, February 2006.

[9] W. Freitas, L.C.P. Da Silva, A. Morelato, 'Small-Disturbance Voltage Stability of Distribution Systems With Induction Generators', IEEE Transactions on Power Systems, Vol. 20, pp. 1653-1654, August 2005.

[10] S. Jang, K. Kim, 'An islanding detection method for distributed generations using voltage unbalance and total harmonic distortion of current', IEEE Transactions on Power Delivery, Vol. 19, pp. 745-752, April 2004.

[11] Z. Ye, A. Kolwalkar, Y. Zhang, P. Du, R. Walling, 'Evaluation of anti-islanding schemes based on nondetection zone concept', IEEE Transactions on Power Electronics, Vol. 19, pp. 1171-1176, September 2004.

[12] F. Katiraei, M.R. Iravani, P.W. Lehn, 'Micro-grid autonomous operation during and subsequent to islanding process', IEEE Transactions on Power Delivery, Vol. 20, pp. 248-257, January 2005.

[13] N. Hatziargyriou, E. Karapidakis, and D. Hatzifotis, 'Frequency stability of power system in large islands with high wind power penetration', Bulk Power Syst. Dynamics Control Symp.-IV Restructuring, Vol. PAS-102, Santorini, Greece, pp. 24-28, August 1998.

[14] Y. Mao, K.N. Miu, 'Switch placement to improve system reliability for radial distribution systems with distributed generation', IEEE Transactions on Power Systems, Vol. 18, pp. 1346-1352, November 2003.

[15] N. Jenkins, R. Allan, P. Crossley, D. Kirschen and G. Strbac, 'Embedded Generation', The Institution of Electrical Engineers, London, United Kingdom, 2000.

[16] N. Hadjsaid, J.F. Canard, F. Dumas, 'Dispersed generation impact on distribution networks', IEEE Transactions on Computer Applications in Power, Vol. 12, pp. 22-28, April 1999.

[17] 'Assessment of Distributed Generation Technology Applications', available at http://www.distributed-generation.com/library.htm, visited on January 2006.

[18] R.C. Dugan, S.K. Price, 'Issues for distributed generation in the US' IEEE Power Engineering Society Winter Meeting, 2002.

[19] J. Machowski, J.W. Bialek, J.R. Bumby, 'Power System Dynamics and Stability', John Wiley & Sons Ltd, 1997.

[20] P. Kundur, J. Paserba, V. Ajjarapu, G. Andersson, A. Bose, C. Canizares, N. Hatziargyriou, D. Hill, A. Stankovic, C. Taylor, T. Van Cutsem, V. Vittal, 'Definition and classification of power system stability, IEEE/CIGRE joint task force on stability terms and definitions', IEEE Transactions on Power Systems, Vol. 19, pp. 1387-1401, August 2004.

[21] P. Kundur, 'Power System Stability and Control', McGraw-Hill, New York, 1994.

[22] 'Analysis and Control of Power System Oscillations', CIGRE Report of Task Force 07, Advisory Group 01, Study Committee 38, December 1996.

[23] E. Handschin, Skriptum zur Vorlesung 'Elektrische Energietechnik 1/2', Dortmund University, WS 1998/1999.

[24] P. Kundur, L. Wang, 'Small signal stability analysis: experiences, achievements, and challenges', IEEE International Conference on Power System Technology, 2002.

[25] Y.V. Makarov, Z.Y. Dong, D.J. Hill, 'A general method for small signal stability analysis', IEEE Transactions on Power Systems, Vol. 13, pp. 979-985, August 1998.

[26] S. Gomes, N. Martins, C. Portela, 'Computing small-signal stability boundaries for large-scale power systems', IEEE Transactions on Power Systems, Vol. 18, pp. 747-752, May 2003.

[27] M. Pavella, P.G. Murthy, 'Transient Stability of Power Systems, Theory and Practice', John Wiley&Sons, 1994.

[28] A.A. Fouad and V. Vittal, 'Power System Transient Stability Analysis: Using the Transient Energy Function Method', Prentice-Hall, 1991.

[29] T.V. Cutsem, C. Vournas, 'Voltage Stability of Electric Power Systems', Kluwer Academic Publishers, 1998.

[30] A. Berizzi, P. Marannino, M. Merlo, M. Pozzi, F. Zanellini, 'Steady-state and dynamic approaches for the evaluation of loadability margins in the presence of secondary voltage regulation', IEEE Transactions on Power Systems, Vol. 19, pp. 1048-1057, May 2004.

[31] Federico Milano, PSAT, http://www.power.uwaterloo.ca/∼fmilano/.

[32] F. Milano, 'An Open Source Power System Analysis Toolbox', IEEE Transactions on Power Systems, Vol. 20, pp. 1199-1206, August 2005.

[33] E.G. Cate , K Hemmaplardh, J.W. Manke, and D.P. Gelopulos, 'Time frame notion and time response of the models in transient, mid-term and long-term stability programs', IEEE Transactions on Power Apparatus and Systems 103(1): 143-151, 1984.

[34] P.W. Sauer, D.J. LaGesse, S. Ahmed-Zaid, and M.A. Pai, 'Reduced Order Modeling of Interconnected Multimachine Power Systems Using Time-Scale Decomposition', IEEE Transactions on Power Systems, Vol. PWRS-2, No. 2, pp. 310-320, May 1987.

[35] V. Venkatasubramanian, H. Schattler, J. Zaborszky, 'Fast time-varying phasor analysis in the balanced 3-phase large electric power system', IEEE Transactions on Automatic Control 40(11): 1975-1982, November 1995.

[36] E.H. Allen, M.D. Ilic, 'Interaction of transmission network and load phasor dynamics in electric power systems', IEEE Transactions on Circuits and Systems I-Fundamental Theory and Applications 47(11): 1613-1620, November 2000.

[37] P.W. Sauer, B.C. Lesieutre, M.A. PAI, 'Transient algebraic circuits for power system dynamic modeling', International Journal of Electrical Power & Energy Systems 15(5): 315-321, October 1993.

[38] P.W. Sauer, M.A. Pai, 'Power System Dynamics and Stability', Prentice-Hall, 1998.

[39] P.M. Anderson, A.A. Fouad, 'Power System Control and Stability', The Iowa State University Press, Volume 1, 1977.

[40] K.R. Padiyar, 'Analysis of Subsynchronous Resonance in Power Systems', Kluwer Academic Publishers, 1999.

[41] P.C. Krause, 'Analysis of Electric Machinery', McGraw-Hill, 1987.

[42] P.M. Anderson, B.L. Agrawal, J.E. Van Ness, 'Subsynchronous Resonance in Power Systems', IEEE Press, 1990.

[43] W.H. Hayt, J.E. Kemmerly, 'Engineering Circuit Analysis', McGraw-Hill, 1993.

[44] W.H. Kersting, 'Radial distribution test feeders', IEEE Power Engineering Society Winter Meeting, 2001.

[45] http://ewh.ieee.org/soc/pes/dsacom/testfeeders.html.

[46] http://www.abb.com/global/abbzh/abbzh251.nsf!OpenDatabase&db=/global/seitp /seitp408.nsf&v=9AAC910040&e=us&c=514877510D363EF7C12570180007CEE3

[47] A. Ramirez, A. Semlyen, and R. Iravani, 'Order reduction of the dynamic model of a linear weakly periodic system-part II: frequency-dependent lines', IEEE Transactions on Power Systems, Vol. 19, pp. 866-871, May 2004.

[48] S. Carneiro, J.R. Marti, 'Evaluation of corona and line models in electromagnetic transients simulations', IEEE Transactions on Power Delivery, Vol. 6, pp.334-342, January 1991.

[49] A. Morched, B. Gustavsen, and M. Tartibi, 'A universal model for accurate calculation of electromagnetic transients on overhead lines and underground cables', IEEE Transactions on Power Delivery, Vol. 14, pp. 1032-1038, July 1999.

[50] T. Noda, N. Nagaoka, and A. Ametani, 'Phase domain modeling of frequency-dependent transmission lines by means of an ARMA model', IEEE Transactions on Power Delivery, Vol. 11, pp. 401-411, January 1996.

[51] H. V. Nguyen, H. W. Dommel, and J. R. Marti, 'Direct phase-domain modeling of frequency-dependent overhead transmission lines', IEEE Transactions on Power Delivery, Vol. 12, pp. 1335-1342, July 1997.

[52] C. Schauder, H. Mehta, 'Vector analysis and control of advanced static VAr compensators', Generation, Transmission and Distribution, IEE Proceedings C, Vol. 140, pp. 299-306, July 1993.

[53] 'Modeling of power electronics equipment (FACTS) in load flow and stability pro-
grams', CIGRE TaskForce 38.01.08, August 1999.

[54] C.A. Canizares, 'Power Flow and Transient Stability Models of FACTS Controllers
for Voltage and Angle Stability Studies', Proceedings of the 2000 IEEE-PES Winter
Meeting, Singapore, January 2000.

[55] H.F. Wang, 'Modelling STATCOM into power systems', International Conference
on Electric Power Engineering, Power Tech Budapest 99, 1999.

[56] R.Mohan Mathur, R.K. Varma, 'Thyristor-Based FACTS Controllers for Electrical
Transmission Systems', Wiley-Interscience, 2002.

[57] X.P. Zhang, C. Rehtanz, B. Pal, 'Flexible AC transmission systems: modelling and
control', Springer-Verlag, 2005.

[58] N. Mohan, T.M. Undeland, and W.P. Robbins, 'Power Electronics, Converters, Ap-
plications and Design (Second Edition)', John Wiley & Sons, New York, 1995.

[59] Q.H. Wu, J.T. Ma, 'Power system optimal reactive power dispatch using evolution-
ary programming', IEEE Transactions on Power Systems, Vol. 10, pp. 1243-1249,
August 1995.

[60] K.Y. Lee, X. Bai, and Y.M. Park, 'Optimization method for reactive power plan-
ning by using a modified simple genetic algorithm', IEEE Transactions on Power
Systems, Vol. 10, pp. 1843-1850, November 1995.

[61] R. Dimeo, K.Y. Lee, 'Boiler-turbine control system design using a genetic algo-
rithm', IEEE Transactions on Energy Conversion, Vol. 10, pp. 752-759, December
1995.

[62] K.Y. Lee, F.F. Yang, 'Optimal reactive power planning using evolutionary algo-
rithms: a comparative study for evolutionary programming, evolutionary strategy,
genetic algorithm, and linear programming', IEEE Transactions on Power Systems,
Vol. 13, pp. 101-108, February 1998.

[63] E. Diaz-Dorado, J. Cidras, E. Miguez, 'Application of evolutionary algorithms for the planning of urban distribution networks of medium voltage', IEEE Transactions on Power Systems, Vol. 17, pp. 879-884, August 2002.

[64] G. Celli, E. Ghiani, S. Mocci, F. Pilo, 'A multiobjective evolutionary algorithm for the sizing and siting of distributed generation', IEEE Transactions on Power Systems, Vol. 20, pp. 750-757, May 2005.

[65] H. Pohlheim, 'Evolutionre Algorithmen. Verfahren, Operatoren und Hinweise fr die Praxis', Springer-Verlag, 1999.

[66] C.M. Hird, H. Leite, N. Jenkins, H. Li, 'Network voltage controller for distributed generation', Generation, Transmission and Distribution, IEE Proceedings, Vol. 151, pp. 150-156, March 2004.

[67] S.N. Liew, G. Strbac, 'Maximising penetration of wind generation in existing distribution networks', Generation, Transmission and Distribution, IEE Proceedings, Vol. 149, pp. 256-262, May 2002.

[68] N.C. Scott, D.J. Atkinson, J.E. Morrell, 'Use of load control to regulate voltage on distribution networks with embedded generation', IEEE Transactions on Power Systems, Vol. 17, pp. 510-515, May 2002.

[69] N.G. Hingorani, L. Gyugyi, 'Understanding FACTS', IEEE Press, New York, 1999.

[70] Y.H. Song, A.T. Johns, Eds., 'Flexible AC Transmission Systems (FACTS)', IEE Press, London, 1999.

[71] Z. Saad-Saoud, M.L. Lisboa, J.B. Ekanayake, N. Jenkins, G. Strbac, 'Application of STATCOMs to wind farms', Generation, Transmission and Distribution, IEE Proceedings, Vol. 145, pp. 511-516, September 1998.

[72] R. Seydel, 'Practical Bifurcation and Stability Analysis, from Equilibrium to Chaos, 2nd Edition', Springer Verlag, 1994.

[73] V. Ajjarapu, C. Christy, 'The continuation power flow: a tool for steady state voltage stability analysis', IEEE Transactions on Power Systems, Vol. 7, pp. 416 - 423, February 1992.

[74] C.A. Canizares, F.L. Alvarado, 'Point of collapse and continuation methods for large AC/DC systems', IEEE Transactions on Power Systems, Vol. 8, pp. 1-8, February 1993.

[75] Hsiao-Dong Chiang, A.J. Flueck, K.S. Shah, N. Balu, 'CPFLOW: a practical tool for tracing power system steady-state stationary behavior due to load and generation variations', IEEE Transactions on Power Systems, Vol. 10, pp. 623-634, May 1995.

[76] X. Zhang, P. Ju, E. Handschin, 'Continuation Three-Phase Power Flow: A Tool for Voltage Stability Analysis of Unbalanced Three-Phase Power Systems', IEEE Transactions on Power Systems, Vol. 20, pp. 1320-1329, August 2005.

Curriculum Vitae

Personal Data:

Born on Oct. 21, 1974, Kunming, P.R. China, Married, Chinese.

Educations:

9/1993 – 7/1997   Bachelor of Science

in the Electrical Engineering Department at Shanghai Jiaotong University, China.

Besides, the second Bachelor Degree specialized in Mechanical Engineering.

9/1998 – 7/2001   Master of Science in Engineering

in the Electrical Engineering Department at Kunming University of Science and Technology, China.

10/2003 – present   PhD student

in Lehrstuhls für Energiesysteme und Energiewirtschaft, Dortmund Universität, Germany.

Work Experience:

8/1997 - 8/1998   Teaching Assistant

in the Electrical Engineering Department at Kunming University of Science and Technology, China

8/2001 - 2/2003   Lecturer

in the Electrical Engineering Department at Kunming University of Science and Technology, China